Cretaceous Research 66 (2016) 60–81

Contents lists available at ScienceDirect

Cretaceous Research

journal homepage: www.elsevier.com/locate/CretRes

Mercury enrichment and Hg isotopes in Cretaceous–Paleogene boundary successions: Links to volcanism and palaeoenvironmental impacts

A.N. Sial [a, *], Jiubin Chen [b], L.D. Lacerda [c], R. Frei [d], V.C. Tewari [e], M.K. Pandit [f], C. Gaucher [g], V.P. Ferreira [a], S. Cirilli [h], S. Peralta [i], C. Korte [d], J.A. Barbosa [j], N.S. Pereira [k]

[a] NEG-LABISE, Department of Geology, Federal University of Pernambuco, Recife, PE, 50740-530, Brazil
[b] State Key Laboratory of Environmental Geochemistry, Institute of Geochemistry, Chinese Academy of Sciences, 46 Guanshui Road, Guiyang, 550002, China
[c] LABOMAR, Institute of Marine Sciences, Federal University of Ceará, Fortaleza, 60165-081, Brazil
[d] Department of Geosciences and Natural Resource Management, University of Copenhagen, Øster Voldgade 10, Copenhagen, 1350 and Nordic Center for Earth Evolution (NordCEE), Denmark
[e] Geology Department, Sikkim University, 6th Mile, Samdur, Tadong Gangtok, Sikkim, India
[f] Department of Geology, University of Rajasthan, Jaipur, 302004, India
[g] Facultad de Ciencias, Universidad de La República, Montevideo, Uruguay
[h] Department of Physics and Geology, University of Perugia, 06123, Perugia, Italy
[i] Instituto de Geología, Universidad Nacional de San Juan-CONICET, 5400, Argentina
[j] LAGESE, Department of Geology, Federal University of Pernambuco, Recife, 50740-530, Brazil
[k] Department of Biology, State University of Bahia, Campus VIII, Paulo Afonso, Brazil

ARTICLE INFO

Article history:
Received 5 February 2016
Received in revised form
19 May 2016
Accepted in revised form 21 May 2016
Available online 27 May 2016

Keywords:
Cretaceous–Paleogene boundary
Chemostratigraphy
Total organic carbon
Molybdenum
Hg isotopes

ABSTRACT

We investigate the use of Hg as a proxy for volcanism by studying four distal and two proximal sections in relation to the Deccan volcanic center, straddling the Cretaceous–Paleogene (KPg) boundary at (a) Højerup (Denmark), Bottaccione and Padriciano (Italy), (b) Meghalaya and Jhilmili (India), and (c) Bajada del Jagüel (Argentina). Hg sequestration by organic matter results in constant Hg/TOC ratio and linear correlation between Hg content of the sediments and total organic carbon (TOC).

Elevated Hg concentrations that deviate from this linear relationship represent most likely true Hg anomalies and these notable Hg/TOC spikes (all TOC <1%) are found in the Meghalaya, Bottaccione and Højerup sections within the CF2 planktic foraminiferal biozone (spike I), at the KPg boundary (spike II), and within the P1a planktic foraminiferal subzone (spike III). Spike III occurs also in the Jhilmili section. No clear correlation between Hg/TOC and Al_2O_3 exists in any of the studied sections. The Hg anomalies probably result from strong volcanic episodes of the Deccan phase-2 (started 250 kyr before the KPg boundary and lasted for 750 kyr) that exhaled sulfuric aerosols, carbon dioxide and other toxic agents which reached a critical threshold, represented in true Hg enrichments in the paleoenvironments. The possibility that Hg enrichments resulted from anoxia scavenging on the seafloor and penetration downward into sediments is not supported in the stratigraphic record of Mo/Al ratios redox proxy.

Hg isotopes were analyzed in samples from all KPg boundary sections in this study and from Bidart, France, the latter for comparison. Hg isotopes yielded δ^{202}Hg values ranging from −1 to −2‰ and Δ^{201}Hg signatures from 0 to 0.05‰ (spike II in Højerup, Bottaccione and Meghalaya KPg boundary layers) consistent with volcanic emission of Hg (0 to −2‰). The δ^{202}Hg in spike I in Meghalaya and Padriciano and spike III in Jhilmili is consistent with volcanic emission of Hg. Two samples from Bajada del Jagüel and four from Bidart, however, display isotope signals compatible with volcanic emission/chondrite Hg. The results of three other samples are characteristic for reworked sediment, soil and/or peat. Most of the data show small positive Δ^{201}Hg, in favor of long-term atmospheric

* Corresponding author. Tel.: +55 81 2126 8243; fax: +55 81 2126 8242.
E-mail address: sial@ufpe.br (A.N. Sial).

http://dx.doi.org/10.1016/j.cretres.2016.05.006

transport prior to deposition, supporting a volcanic origin for the Hg. The present study broadens, therefore, the potential use of Hg as stratigraphic marker and, moreover, confirms that in the critical KPg transition, Hg was enriched in paleoenvironments at three distinct stages during the Deccan phase-2.

1. Introduction

Volcanic emissions have the potential of injecting large amounts of Hg into the atmosphere and, therefore, contribute with a significant natural input of Hg to the atmosphere (e.g. Schuster et al., 2002; Pyle and Mather, 2003). Many studies have reported Hg enrichments in sedimentary records that are synchronous with modern (e.g. Martínez-Cortizas et al., 1999; Roos-Barraclough et al., 2002; Roos-Barraclough and Shotyk, 2003) and prehistoric volcanic events (e.g. Palinkaš et al., 1996; Sial et al., 2010, 2013, 2014; Nascimento-Silva et al., 2011, 2013; Sanei et al., 2012; Grasby et al., 2013, 2015a, 2015b; Percival et al., 2015; Font et al., 2016). In contrast to most elements present in ash, Hg derived from volcanic activity is mainly in gaseous form (Hg^0), can be transported far in the atmosphere, reaching even global-scale distribution prior to deposition in terrestrial and marine environments and has a long atmospheric residence time (1–2 years). Through oxidation in the atmosphere, Hg^0 forms reactive Hg^{+2}, soluble in water and, therefore, enriched in the rain (e.g. Schroeder and Munthe, 1998; Witt et al., 2008 and references therein). Organic matter and clay minerals scavenge Hg in the marine environment and fix it in bottom sediments on the sea floor (Grasby et al., 2015a; Percival et al., 2015).

If Hg reaches an environment with low organic scavenging capacity on the surface, then Hg^{+2} remains in solution and is, eventually, adsorbed onto clays and transported from land to sea. Therefore, high levels of Hg associated with argillaceous sediments can be explained by increased flux of volcanogenic Hg from continents into the oceans. Higher Hg accumulation rates are typical and more pronounced in sediments deposited after glacial maxima, when runoff is increased, compared to sediment layers deposited before such events. This peculiarity is perhaps a phenomenon that can be observed globally as similar results have been observed in the Amazon region (Santos et al., 2001), Antarctica (Vandal et al., 1993) and Europe (Martínez-Cortizas et al., 1999). Biotic or abiotic reduction of Hg^{2+} to Hg^0 (g) limits the scavenging and biological fixation of Hg from the atmosphere and, in consequence, allows Hg re-emission and higher concentration in the atmosphere (Percival et al., 2015). Under reduced bioproductivity, Hg availability stops being captured by organic matter which is one of the major Hg sinks (Sanei et al., 2012).

A strong linear correlation between Hg and total organic matter (TOC) contents in sediments and an apparent affinity of Hg for terrestrial organic matter has been recognized (Outridge et al., 2007; Stern et al., 2009; Sanei et al., 2014) but the importance of terrestrial versus aquatic retention of Hg is still an open question (Percival et al., 2015). Increased Hg concentrations in sediments that deviate from a linear relationship between Hg and TOC represent true Hg anomalies. On the other hand, Hg can be adsorbed onto clays (Krupp, 1988). In this case one would expect a covariation between Hg and Al_2O_3, as for example observed in some sections across the KPg boundary (e.g. Sial et al., 2013).

It has also been suggested that Hg emission rates can be significantly enhanced in periods of large igneous province (LIP) volcanic activity when the marine buffering control on Hg can be overwhelmed and thus generating Hg spikes in sediments (Sanei et al., 2012; Grasby et al., 2013, 2015a; Font et al., 2016). Therefore, Hg anomalies could serve as proxy for periods of extensive volcanic activities when LIPs, for example, could have released toxic quantities of Hg into environment. The Hg flux to the sedimentary realm accompanying large amounts of magmatic sulfur and other toxic metals released by LIPs (e.g. Deccan Traps, Callegaro et al., 2014) can provide missing links between the terrestrial and marine records of biota extinctions as suggested by Grasby et al. (2015a).

Sanei et al. (2012) related enhanced atmospheric Hg depositions at the Permian–Triassic transition to catastrophic volcanic eruptions of the Siberian Trap LIP event, followed by the discontinuity of the organic Hg fixation that lead to an increased dissolved Hg flux. The Permian–Triassic biotic crisis, as well as the extinction events in the late Capitanian and at the Smithian/Spathian boundary in NW Pangea, has been linked to enhanced Hg deposition (Grasby et al., 2013, 2015a, 2015b). In addition, the end-Pliensbachian extinction and Toarcian oceanic anoxic event (OAE) are probably related to LIP activities (Karoo–Ferrar), according to Percival et al. (2015). Acidic rain has been deemed responsible for the mass extinction associated to the KPg boundary (Hsü and McKenzie, 1985) and Hg enrichments in KPg boundary sedimentary rocks have been regarded as an evidence for this type of rain (Hildebrand and Boynton, 1989). Anomalous Hg concentrations in deposits spanning the KPg boundary in Dolenja Vas, Slovenia, likely resulted from sub-aerial volcanic activity (Palinkaš et al., 1996).

Subsequent work suggested a possible connection between enhanced Hg concentrations in sedimentary rocks across the KPg boundary and Deccan Traps events (Nascimento-Silva et al., 2011, 2013; Sial et al., 2013, 2014) and enabled a distinction of chemical fingerprints related to the Deccan volcanism from an impact event at the KPg boundary (Sial et al., 2014). However, these studies have not taken the mutual relationship between TOC content and Hg concentrations into account, and this precludes an evaluation on how lithological variation (organic matter-poor versus organic matter-rich sediments) was related to the reported Hg anomalies.

Post-emission or post-discharge Hg transformations may not drastically modify the isotopic composition of particulate Hg according to several authors (e.g. Foucher et al., 2009; Sonke et al., 2010; Estrade et al., 2011; Gehrke et al., 2011; Chen et al., 2012; Sun et al., 2013). When Hg transformations lead to change of Hg isotope signatures, this change tends to be constant under certain conditions (Laffont et al., 2009, 2011; Gehrke et al., 2011). Multiple Hg transformations may modify the Hg isotope signatures in unpredictable way, making difficult to trace the Hg source (Sonke and Blum, 2013).

The Hg isotopic composition may help in the distinction between volcanogenic and meteoritic Hg. It is not simple to precise the isotope composition of mantle-derived Hg because usually it is not entirely mantle-derived and/or because it has undergone fractionation during chemical/phase transformation at near surface regions (Bergquist and Blum, 2009). Mantle-derived Hg probably has δ^{202}Hg values close to 0‰ according to Sherman et al. (2010), but Zambardi et al. (2009) have reported values from −1.74‰

to −0.11‰ for gas and particulates, respectively, from an active volcano in Italy. Generally, geogenic Hg does not have significant mass independent fractionation (MIF) of odd Hg isotopes (Δ^{201}Hg or Δ^{199}Hg) (Blum et al., 2014). On the other hand, Hg in most natural samples displays δ^{202}Hg values significantly different from crust and mantle values after it has undergone cycling in the surface environment (Bergquist and Blum, 2009). Interestingly, these samples commonly have significant MIF signatures as a result of photoreactions (or evaporation), with generally negative Δ^{201}Hg for surface soils, sediments and land plants, while positive Δ^{201}Hg values are observed for precipitation, aquatic organisms and atmospheric particles (Blum et al., 2014). Hg isotopes are potentially able to discriminate natural from anthropogenic Hg sources (Sonke and Blum, 2013).

2. The Deccan province and the KPg boundary event

Continuous advances in radiometric age dating have gradually confirmed the ties between the Kalkarindji, Viluy, Siberian, Central Atlantic magmatic province, and Deccan volcanism to the Early–Middle Cambrian (Jourdan et al., 2014), end-Devonian, end-Permian, end-Triassic, and end-Cretaceous mass extinctions, respectively (Keller and Kerr, 2014). In the Deccan lavas which flooded the Indian subcontinent (Raja Rao et al., 1999), three phases of continental flood basalts are known (e.g. Chenet et al., 2009) with a total of 6% volume erupted in phase-1 (C30n–C31n), while 80% was erupted in phase-2 (C29r), and 14% in phase-3 (C29n). An about 850,000 years quiescence of Deccan volcanism separated Deccan phase-1 from phase-2. Phase-2, the longest lava flows in the Phanerozoic (Self et al., 2008) started at 66.288 ± 0.027 Ma (U–Pb zircon dating; Schoene et al., 2015), preceding the KPg boundary (65.968 ± 0.085 Ma; Renne et al., 2013) with around 250,000 years, encompassing the age interval of the CF2 and CF1 planktic foraminifers biozones. Deccan phase-2 ended at 500,000 years after the KPg boundary (65.552 ± 0.026 Ma). About 1.1 million km^3 of lavas were erupted (Schoene et al., 2015). Deccan Traps eruptions have been blamed responsible for the mass extinction documented in the intertrappean beds in India (e.g. McLean, 1985; Keller et al., 2011, 2012, and references therein).

It is known that volcanic gases (e.g. CO_2 and SO_2) from a single eruptive event, and not the total volume erupted, may cause devastating impacts on Earth's environment and life (Svensen et al., 2009; Bond and Wignall, 2014). The Deccan Traps contain magmatic sulfur concentrations as high as 1900 ppm (Callegaro et al., 2014), much higher than in basalts from some other similarly sized igneous provinces (e.g. Paraná–Etendeka). Therefore, eruptions likely caused globally extensive acidic rains before and during the KPg boundary, resulting in weathering and dissolution effects on land. Dissolution of foraminifers (e.g. Gertsch et al., 2011) and of iron oxide minerals (bio- and detrital magnetite) is may be considered as important evidence of acidification of oceans during this critical period (Font et al., 2014). Punekar et al. (2014) investigated the environmental/biological effects of the Deccan Traps eruptions using C and O isotopes and demonstrated that the global high-stress environment prior to the KPg boundary is coeval with the Deccan eruption phase-2 in C29r. These authors have also concluded that the Deccan phase 3 correlates with the delayed Danian biotic recovery in C29n. Keller et al. (2016) reviewed the chronology and geographic distribution of the three Deccan phases in India. It is not yet possible to precisely date the Deccan flood basalts associated with mass extinction. Therefore, one cannot yet quantify the effects of volcanism and asteroid impact on the KPg boundary mass extinction. In the present study, we use Hg, as tracer in order to investigate the influence of distal volcanism, in worldwide chemostratigraphic profiles across the KPg boundary with the overall aim to contribute to solve this problem.

3. Study aims

The present study aims at: (a) broadening the knowledge and contrasting Hg spikes (Hg/TOC) as volcanogenic signals in marine sediments in sections straddling the boundary from different continents to confirm the global extent of Hg loading related to the Deccan Traps volcanism, and (b) examining Hg isotopes from these sites to help telling apart influence of volcanism from bolide impact fingerprints in KPg events. By examining these Hg stratigraphic patterns, we investigate worldwide fingerprints of Deccan eruptions in climate change.

4. Study areas

Four distal KPg boundary sections relative to the Deccan Traps volcanic center (Denmark, Italy and Argentina) and two proximal sections (India) are the focus of this study (Fig. 1). They represent well-documented sites in the Northern Hemisphere (Højerup at Stevns Klint, Bottaccione at Gubbio and Padriciano near Trieste), and in the Southern Hemisphere (Meghalaya, Jhilmili and Bajada del Jagüel). Mercury chemostratigraphical data from the Højerup, Bottaccione, and Bajada del Jagüel sections are found in Sial et al. (2014), who have not reported TOC% values alongside with Hg concentrations. This lack of TOC data has limited the further use of the depicted Hg spikes as proxy for volcanism. No Hg chemostratigraphy has been so far reported for the Padriciano section, a classical shallow-marine carbonate platform (Trieste Karst, Italy), for Meghalaya, South Shillong Plateau (NE India) and for the Jhilmili section (central India). The last two sections are located at proximal and very proximal distances to the Deccan volcanic province, respectively, and are of paramount importance for the assessment of Hg as fingerprint of eruptions in the period of the end-Cretaceous mass extinction.

In selecting sections for this study, we paid much attention to stratigraphic completeness of the sedimentary successions and the geographic distribution of the sites. It is known that the sections at Højerup (Stevns Klint), Bottaccione (Gubbio) and Meghalaya sections, based on the study of planktic foraminiferal biozones, are likely complete. Stevns Klint is the best preserved and laterally the most extensive KPg succession (UNESCO World Heritage Site, since June 2014). All foraminiferal biozones are present in the uppermost Maastrichtian to lowermost Danian succession at Højerup (Rasmussen et al., 2005; Surlyk et al., 2006; Thibault et al., 2015).

Refined magnetostratigraphy, planktic foraminiferal and calcareous nannofossil biostratigraphies are available for the stratigraphic succession at Gubbio (e.g. Coccioni et al., 2010; Coccioni and Premoli Silva, 2015). These authors have reported the presence of CF1, CF2 and CF3 foraminiferal biozones in the uppermost Maastrichtian, encompassing the Scaglia Bianca and Scaglia Rossa formations up to the KPg boundary. In the Shillong Plateau, seven successive planktic foraminiferal biozones from across the KPg boundary at the Um Sohrynkew section (Meghalaya) are present (Mukhopadhyay, 2008; Pal et al., 2015) and these are in stratigraphic order CF4, CF3, CF2 and CF1 in the upper Maastrichtian part and the P0 and Pα zones and P1a subzone in the lower Danian part, representing a biostratigraphically continuous record across the KPg boundary. The Jhilmili intertrappean beds record the lower Danian (planktic foraminifers P1a subzone; Keller et al., 2009) and represent the closest section to the Deccan volcanic center.

In the Bajada del Jagüel section, Neuquén Basin, the CF1 biozone and the base of the Danian (P0, P1a, P1b) seem to be missing (Keller

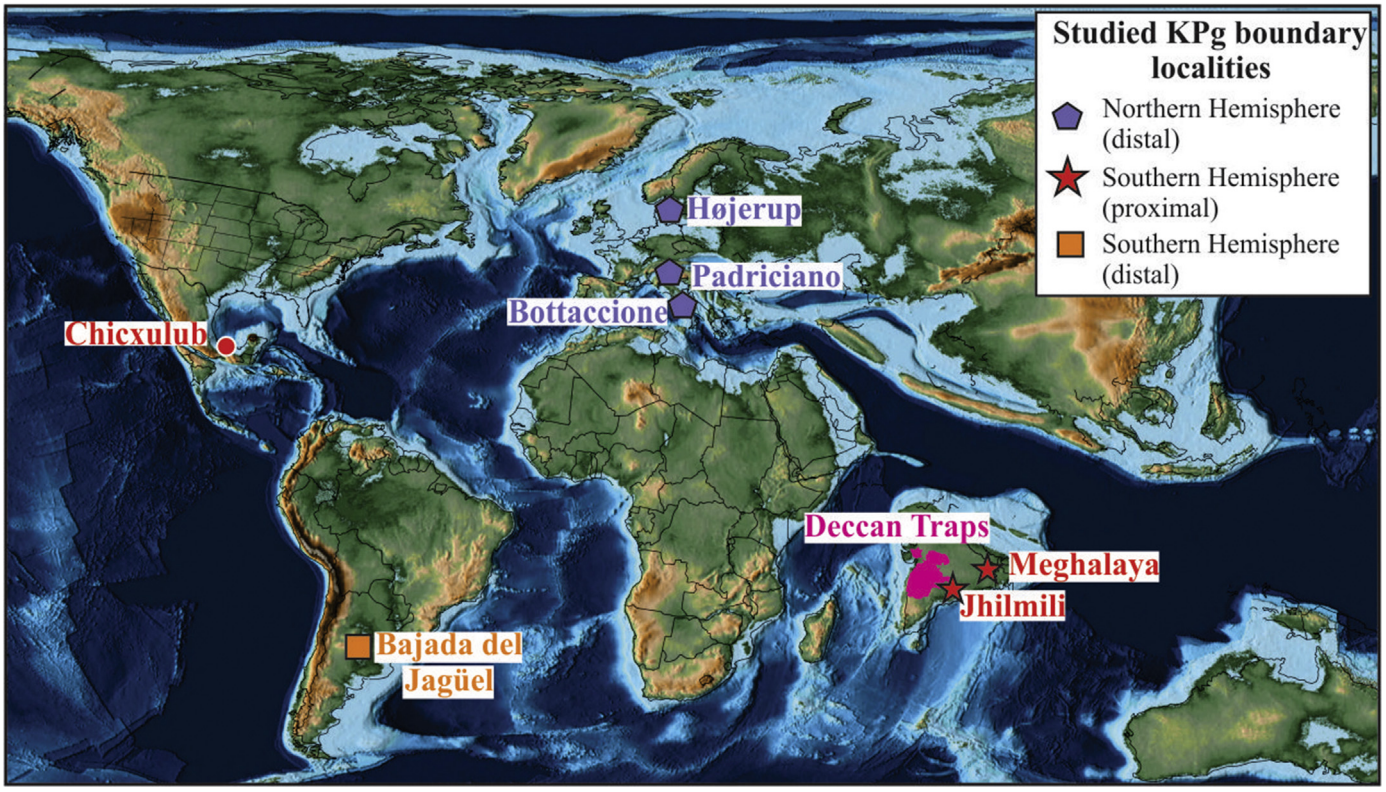

Fig. 1. Paleomap at 66 Ma showing paleogeography and location of the studied KPg boundary sections (based on Scotese, 2013). The location of the Chicxulub impact structure is indicated. Colored stars mark the three distinct types of studied KPg boundary sections in relation to the Deccan volcanic province center: (A) Northern Hemisphere (distal >5000 km); yellow; (B) Southern Hemisphere (proximal to very proximal; up to 1000 km); red; (C) Southern Hemisphere (distal > 5000 km); orange. (For interpretation of the references to color in this figure legend, the reader is referred to the web version of this article.)

et al., 2007; Pardo and Keller, 2008). The latest Maastrichtian association of planktic foraminifers is composed of species which are not age-diagnostic and, therefore, it is not possible to precisely pinpoint the exact biozones at this site. The absence of typical species of the CF1 zone led Keller et al. (2007) to tentatively assign the latest Maastrichtian foraminifers in the Bajada del Jagüel section to the CF2 zone. Typical Danian species occurring at the base of the Pα zone (*P. eugubina* or *P. longiapertura*) seem to be absent.

Palamarczuk et al. (2002) have mentioned co-occurrence at Bajada del Jagüel section, of dinoflagellate (*Senoniasphaera inornata* and *Damassadinium californicum*) and foraminifers (*Guembelitria cretacea* and *Hedbergella montmouthensis*) within the KPg boundary sandstone and in foraminiferal zone Pα (*P. eugubina*) above, suggesting that this 20 cm-thick sandstone which marks the KPg transition lies within Zone P0. Besides, according to Palamarczuk et al. (2002), the 50 cm interval directly above the sandstone contains planktic foraminiferal species typical of zones Pα through P1c. An $^{40}Ar/^{39}Ar$ plateau age of 66 ± 0.5 Ma for feldspar from the KPg boundary ash bed was reported by the same author. Habib and Saeedi (2007) have recognized an abundance of *Manumiella seelandica* (dinoflagellate) immediately below the KPg boundary and stated that the global distribution of this species makes it an excellent biostratigraphic marker. Fossils of *M. seelandica* have been reported from mid-latitude sites in Argentina (Palamarczuk and Habib, 2001; Palamarczuk et al., 2002). The pattern of magnetic susceptibility for the sedimentary rocks across the KPg boundary suggests that the section at Bajada del Jagüel is incomplete with respect to the very uppermost Maastrichtian, although the time span of interest may be as short as 40 kyr (Nañez et al., 2002). Aberhan et al. (2007) found neither a sign of the Danian planktic foraminiferal zone P0 nor impact specific trace element concentrations in the KPg boundary sandstone layer in the Bajada del Jagüel section, and concluded that this succession lacks about 100 kyr of a sedimentary depositional period. The disagreement about how much of sedimentary record is missing in the Bajada del Jagüel section can be somehow addressed and tested by comparing the episodic distribution of Hg/TOC anomalies with those in more complete sections as done here.

4.1. The Danish Basin, Stevns Klint, Denmark

The Stevns Klint (coastal cliffs) is located about 45 km south of Copenhagen, Denmark, on the island of Sjælland (Figs. 1, 2). The sediments, deposited in the Danish Basin, represent one of the most complete KPg boundary section worldwide. They exhibit a KPg boundary layer beneath a topographic overhang separating the lowermost Danian Cerithium Limestone Member from the overlying lower Danian bryozoan limestone of the Stevns Klint Formation (Fig. 8; Surlyk, 1997; Surlyk et al., 2006, 2013). The distinct boundary clay (Fiskeler Member) varies in thickness and is mainly around 5 cm, but up to 40 cm at Kulstirenden, in the northernmost part of the cliff, including here the so-called 'red layer' just above its base (Hart et al., 2004). There is clear evidence for shallowing in the latest Maastrichtian before the KPg boundary, and for sea-water temperature fluctuations (Surlyk, 1997; Hart et al., 2004; Thibault et al., 2015).

The 45 m-thick succession exposed at Stevns Klint exhibits the stratigraphic evolution of the Danish Basin from the latest Cretaceous, across the KPg boundary into the early Paleogene. The most comprehensive stratigraphic studies of these sections are those of Surlyk (1997), Rasmussen et al. (2005); Surlyk et al. (2006; 2013). At the Højerup coastal cliff section, the Maastrichtian Møns Klint

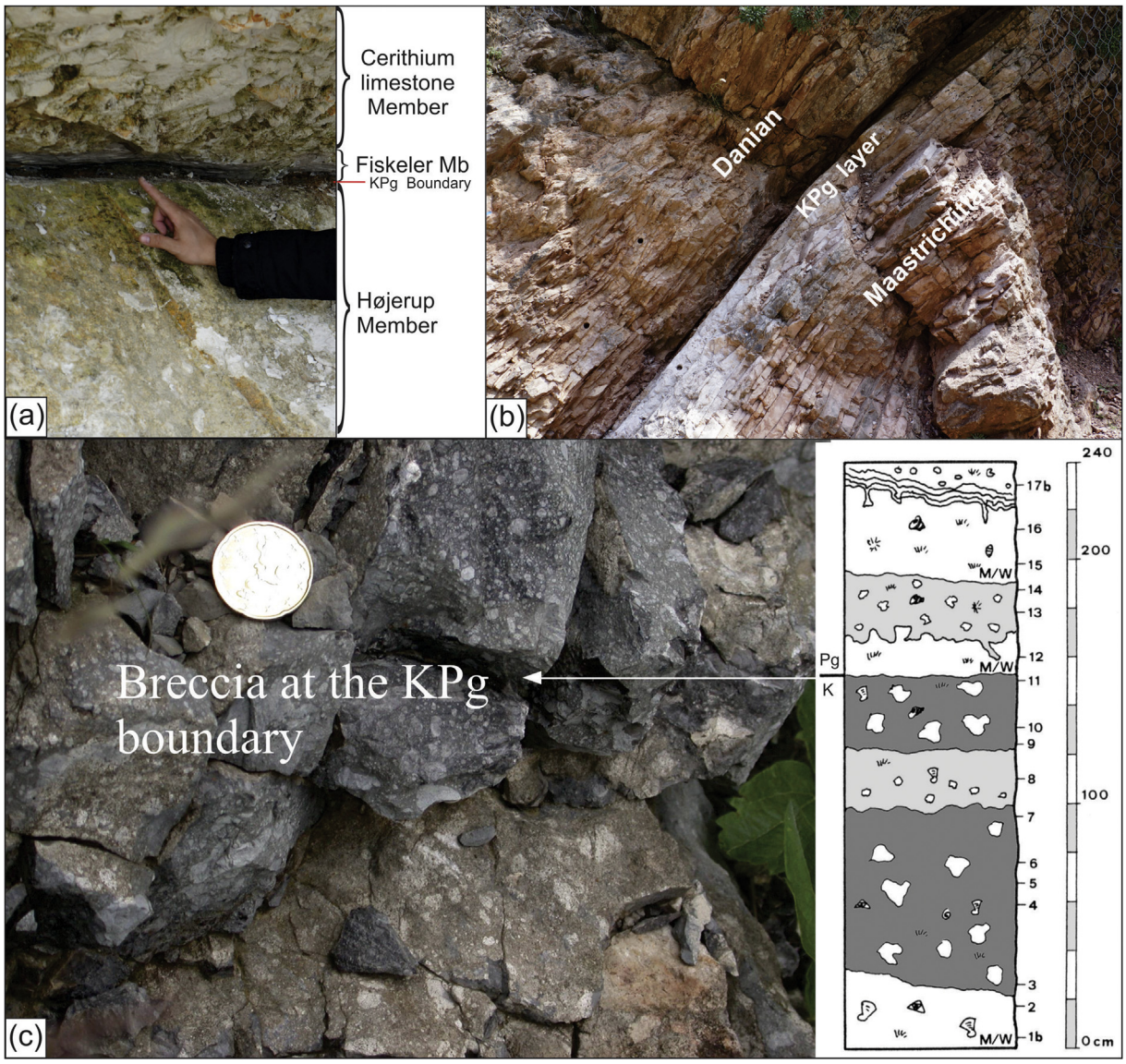

Fig. 2. (A) Closer view of the KPg boundary layer (Fiskeler Member) in the Højerup section, Stevns Klint, Denmark; (B) KPg boundary layer (1–2 cm thick) within the Scaglia Rossa Formation at the Bottaccione Gorge, near Gubbio, Italy; (C) Closer view of the upper breccia level at the KPg boundary in Padriciano, near Trieste, Italy.

Formation (Sigerslev and Højerup members; Surlyk et al., 2013; Hansen and Surlyk, 2014) is overlain by the lower Danian Rødvig Formation (Fiskeler and Cerithium Limestone members) which in turn is covered by the lower to middle Danian Korsnæb Member of the Stevns Klint Formation (Surlyk et al., 2006). The Cerithium Limestone is diachronous and becomes gradually younger from the southern part of Stevns Klint towards the northern part. A hiatus including all the *P. eugubina* zone is present at the Fiskeler–Cerithium Limestone transition in the northern part of the cliff but it is absent in the southern part (Rasmussen et al., 2005). Danian bryozoan limestone mounds, outlined by black flint bands, formed shortly after the KPg boundary mass extinction (Lauridsen et al., 2012 and references therein).

4.2. The Umbria–Marchean succession, Central Apennines, Italy

The Gubbio Mountains are part of the Umbria–Marche Basin with two well-known KPg boundary sections (Figs. 1, 2 and 8B). These occur in two parallel valleys, the Bottaccione Gorge and the Contessa Highway. The former begins just outside the town of Gubbio and cuts through pelagic Middle Jurassic to upper Eocene sedimentary rocks, including the Calcari Diasprigni, Maiolica, Marne a Fucoidi formations and the Scaglia Group (Scaglia Bianca, Scaglia Rossa, Scaglia Variegata and Scaglia Cinerea formations). The Bottaccione section represents the magnetostratigraphic standard for the Upper Cretaceous–Eocene interval (e.g. Galeotti et al., 2015) and contains a 1 cm-thick clay layer at the KPg boundary (Fig. 2) within the Scaglia Rossa Formation, enriched in Ir (Alvarez et al., 1980). In contrast to Stevns Klint, the KPg boundary layer at Gubbio has a very short lateral extent as the succession is tilted (Fig. 2B).

Alternation of gray and pink colored beds marks the contact between the Scaglia Bianca and the overlying Scaglia Rossa formations. The latter brackets the KPg boundary and consists of predominantly pink to red pelagic limestones with cherty nodules and calcareous marls, with bedding thicknesses between 10 and 20 cm. This Upper Cretaceous to lower middle Eocene succession represents an apparently continuous stratigraphic record across the

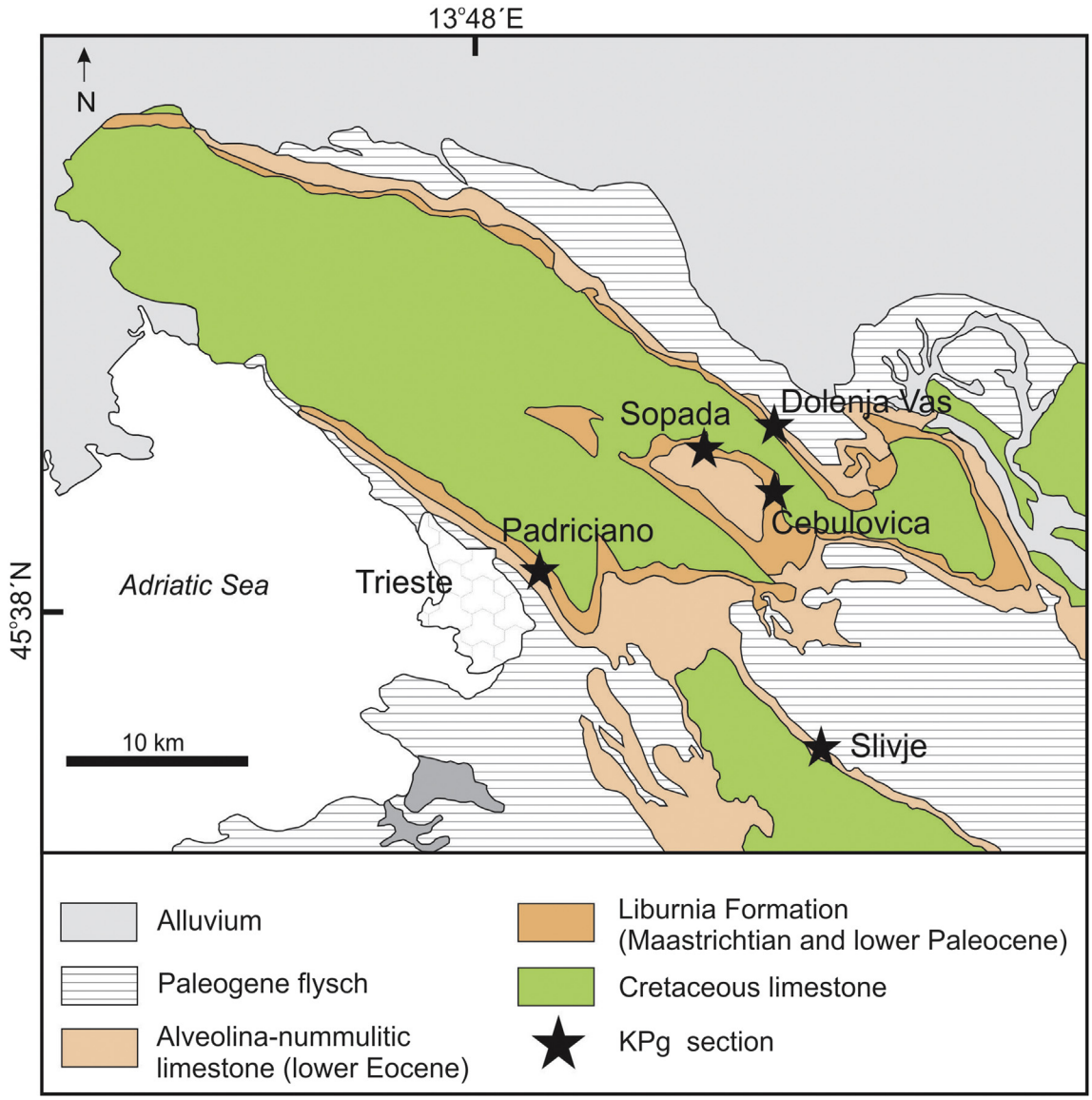

Fig. 3. Summary geological map showing five sites of studied KPg boundary sections in the Trieste Karst region of Slovenia and northeastern Italy (modified from Pugliese et al., 1995). Black stars mark the location of KPg boundary sections.

KPg boundary and based on abundant planktic and benthic foraminifers and calcareous nannofossils, it has been dated as Late Cretaceous to early middle Eocene (Premoli Silva and Sliter, 1994; Alvarez, 2009; Coccioni and Premoli Silva, 2015 and references therein).

The KPg boundary crops out on the eastern side of the main road and lies around 240 m above the base of the Scaglia Rossa Formation (Figs. 2B, 8B). The topmost Cretaceous in this section is represented by a 30–40 cm-thick whitish limestone bed, overlain by the 2 cm-thick dark clay KPg boundary layer which correlates to the well-known KPg boundary mass-extinction event (Premoli Silva and Sliter, 1994). The lowermost Paleocene is correlated with the occurrence of *Globigerina eugubina* foraminiferal zone (=*Parvorugoglobigerina eugubina*; Luterbacher and Premoli Silva, 1964).

4.3. The Trieste Karst, NW Adriatic platform, Italy

The Karst region including the Trieste area of Italy and a portion of Slovenia is part of the Adriatic platform and is characterized by Maastrichtian to Danian peritidal carbonate deposits (Fig. 3). In Italy, the thickest succession of this shallow carbonate platform is located at Padriciano (Fig. 3). In the Trieste Karst, the KPg boundary is well-documented in some sections at Padriciano (Pugliese et al., 1995, 2000; Tewari et al., 2007). The interval including the KPg boundary is characterized by presence of several peritidal cycles consisting of basal breccias, lagoonal limestone, and stromatolitic limestone with typical fenestral fabric.

The KPg boundary in the carbonate platform of the Karst region of Slovenia was first identified by Drobne et al. (1989). The main criteria they used to identify the KPg boundary was by the occurrence of certain biota, particularly by the disappearance of Cretaceous taxa and appearance of Paleogene ones, by identification of foraminiferal zone SBZ1 and of magnetic polarity Ch29r, the presence of and Ir anomaly and by the strong negative shift of $\delta^{13}C$ values across the KPg boundary (Hansen et al., 1995; Marton et al., 1995; Ogorelec et al., 1995; Hansen and Toft, 1996; Palinkaš et al., 1996). The same criteria have been adopted for locating the KPg boundary in the Trieste Karst and, in addition, the presence of microtektites at the top of a Maastrichtian breccia near the village

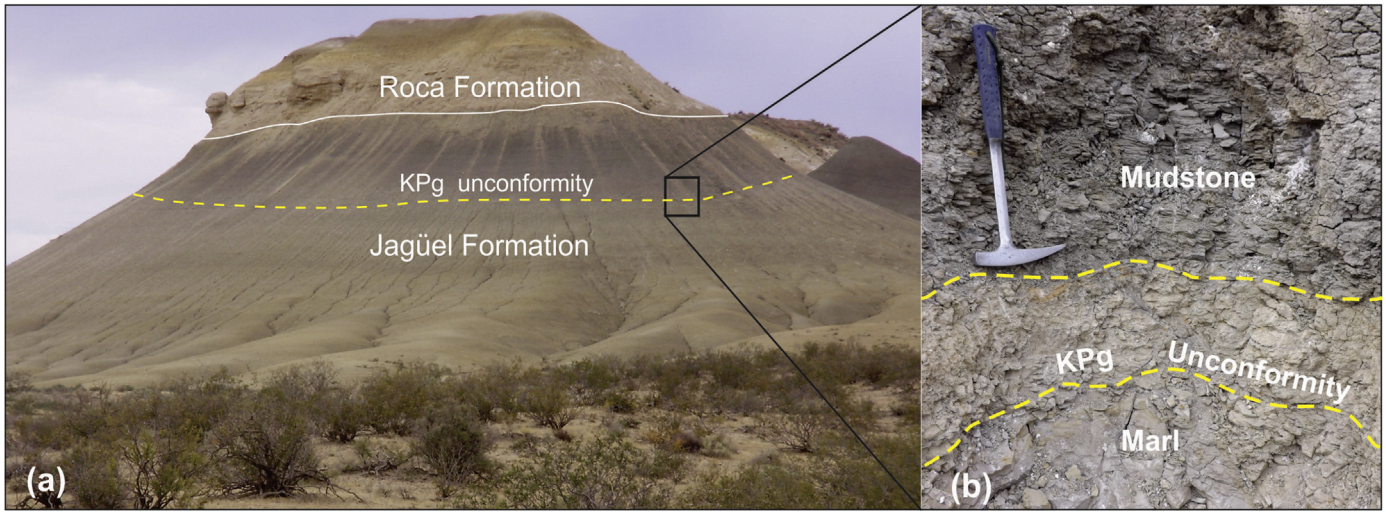

Fig. 4. Yellow volcanoclastic sandstone layer (20 cm thick) marking the KPg boundary in the Bajada del Jagüel section, Neuquén Basin, Argentina. (For interpretation of the references to color in this figure legend, the reader is referred to the web version of this article.)

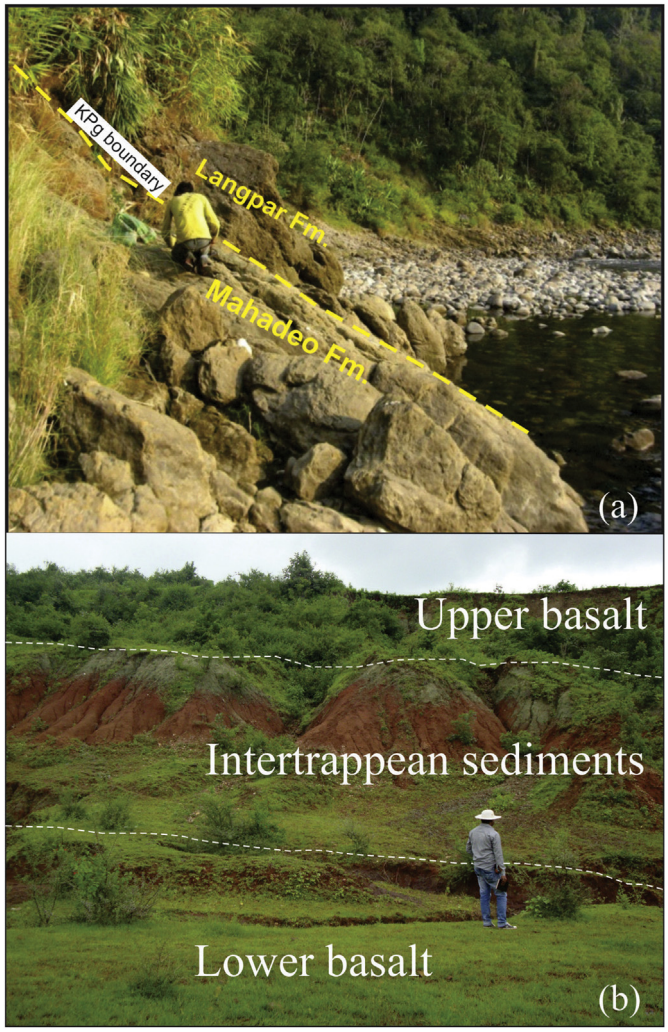

Fig. 5. Field aspects of the two sampled sections in India: (A) KPg boundary location between the Mahadeo and Langpar formations in an Um Sohrynkew River section, not far from Theria village, Shillong Plateau, northeastern India; (B) Jhilmili section showing the two basalt traps and sandwiched intertrappean sedimentary rocks.

of Padriciano was also regarded as evidence for the record of the KPg boundary in this region (Gregorič et al., 1998).

The peritidal shallow carbonate succession at Padriciano is represented by the Liburnia Formation (Fig. 3) which contains a Maastrichtian breccia (50 cm-thick, Fig. 2), another breccia (20 cm-thick) of dark limestone with rudist shell fragments and foraminifers (Tewari et al., 2007) about 80 cm below the upper breccia (Fig. 2). The KPg boundary is situated at the base of the upper breccia, the latter overlain by a succession of light gray Danian limestone with *Microcodium* that is overlain by stromatolitic limestone also with *Microcodium*. A change in the foraminifer species from Miliolidae, *Rhapydionina liburnica, Fleuyriana adriatica* to the occurrence of *Microcodium* and *Bangiana hanseni* is present immediately below the upper breccia (Caffau et al., 1998). This brown limestone, with gastropod fragments and *Microcodium*, is overlain by gray stromatolitic limestone capped or penetrated by *Microcodium*. Further peritidal cycles of gray limestone overlain by stromatolitic limestone with *Microcodium*, forming thick units, follow up-section. Within lagoonal limestones of these cycles, some Danian opportunistic and r-strategist foraminifers taxa (e.g. *Bangiana hanseni* and small Miliolidae) appear (Pugliese et al., 2000; Tewari et al., 2007) and characterize the Danian larger benthic foraminiferal zone 1 (SBZ 1; Serra-Kiel et al., 1998) which corresponds to the planktic foramineral P0, Pα and P1 biozones of Berggren et al. (1995).

4.4. The Neuquén Basin, Patagonia, Argentina

The Neuquén Basin in Patagonia of western Argentina is located between 32° and 40°S latitude on the eastern side of the Andes in Argentina and central Chile. This foreland basin comprises Upper Triassic to Miocene deposits (Vergani et al., 1995; Legarreta and Uliana, 1999; Howell et al., 2005). The KPg transition is situated in the Upper Cretaceous–lower Paleocene Malargüe Group that comprises the Allen, Jagüel, Roca and El Carrizo formations and deposited unconformably overlying the Upper Cretaceous Neuquén Group (Legarreta et al., 1989; Casadío, 1998; Heredía and Salgado, 1999).

The KPg transition in this basin has been extensively investigated by biostratigraphy, microfacies analysis, bulk rock/clay mineralogy, isotope stratigraphy, and trace and major element chemistry (e.g. Howell et al., 2005; Scasso et al., 2005; Aberhan et al., 2007; Keller et al., 2007; Musso et al., 2012). These and further results show

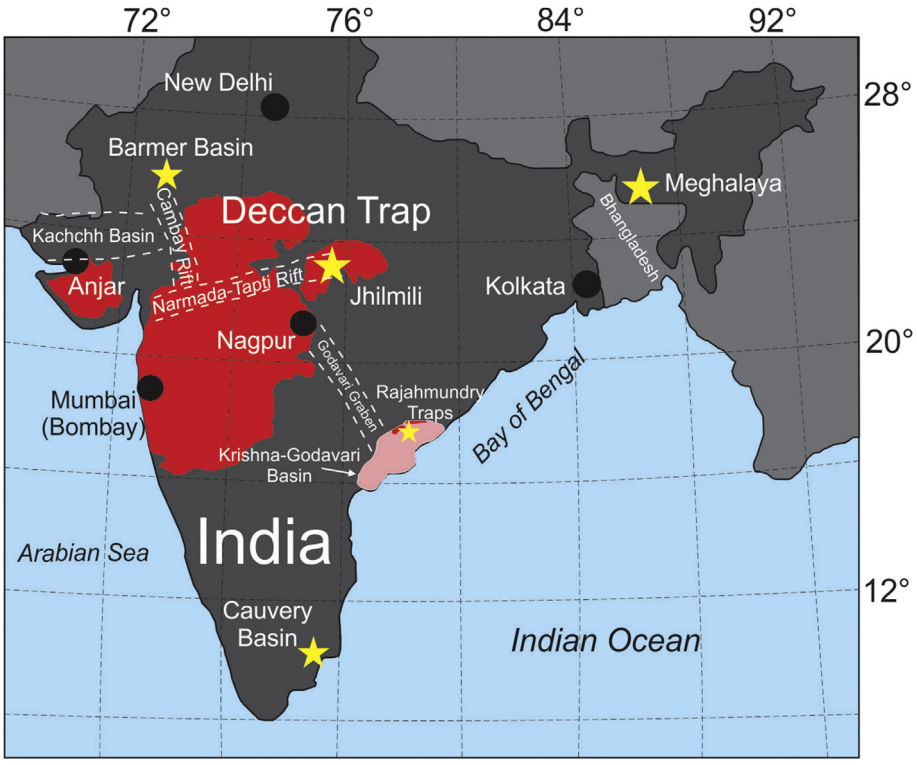

Fig. 6. Geographic map of India showing the location of well-known KPg boundary sections, marked by stars (Meghalaya, Jhilmili, Anjar, and Barmer, Krishna–Godavari and Cauvery basins). Also shown in this map is the Deccan volcanic province and the extent of the Narmada–Tapti seaway (modified from Cripps, 2002; Shukla and Srivastava, 2008; Keller et al., 2009).

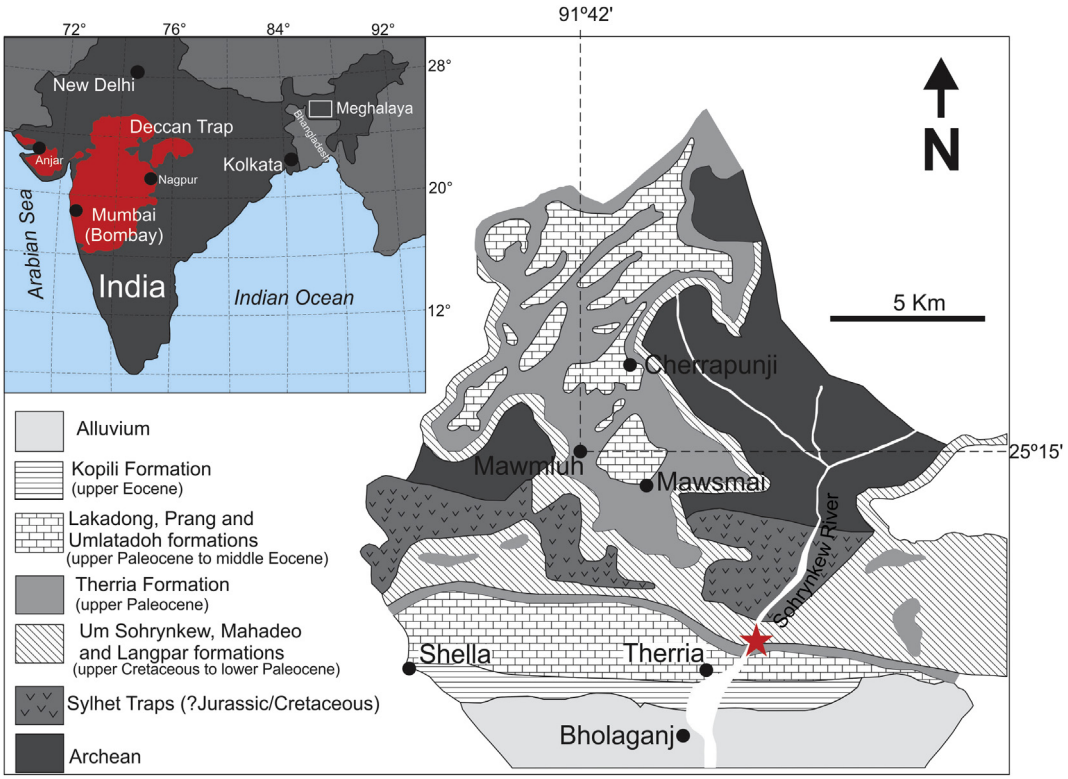

Fig. 7. Summary geological map of South Shillong Plateau, Meghalaya, northeastern India (modified from Tewari et al., 2010a, 2010b). Star indicates locality of the sampled section.

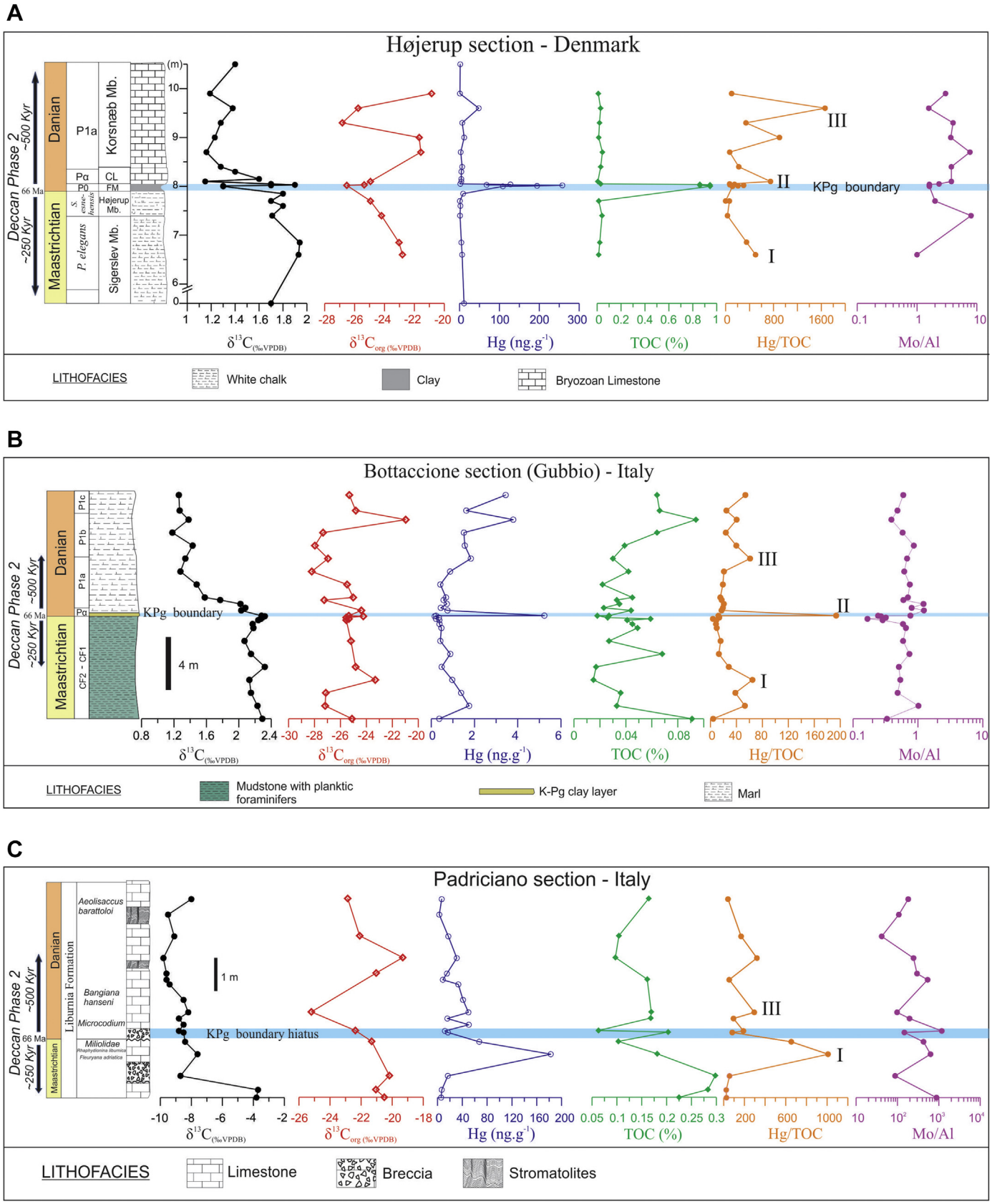

Fig. 8. (A) $\delta^{13}C_{carb}$, $\delta^{13}C_{org}$, Hg/TOC and Mo/Al variation patterns across the KPg boundary at Højerup, Stevns Klint (Maastrichtian planktic foraminiferal biostratigraphy from Surlyk et al., 2006, and Danian, from Rasmussen et al., 2005); (B) Bottaccione (Gubbio) section (planktic foraminiferal biostratigraphy from Coccioni et al., 2010; Coccioni and Premoli Silva, 2015) and (C) Padriciano section (foraminiferal biostratigraphy from Tewari et al., 2007), Italy.

that the Maastrichtian succession was deposited during transgression. A regressive trend was recorded in the Paleocene (Scasso et al., 2005; Aguirre-Urreta et al., 2011). The Jagüel Formation encompasses the KPg boundary (e.g. Uliana and Biddle, 1988) and consists of 90-m thick, monotonous marine mudstones deposited in a mid-to outer-shelf environment, covered by bioclastic marine limestones of the Danian Roca Formation (Fig. 4). The KPg boundary interval has been identified on the basis of palynomorphs (Papú et al., 1999), ostracods (Bertels, 1975), calcareous nannofossils and foraminifers (Nañez and Concheyro, 1997). The position of the KPg transition is constrained to a single, thin coarse-grained sandstone bed (Palamarczuk and Habib, 2001; Palamarczuk et al., 2002; Scasso et al., 2005) in the upper half of the Jagüel Formation, and Danian age above has been confirmed by calcareous nannofossils (Scasso et al., 2005). This 15–25 cm thick non to slightly lithified tuffaceous sandstone can be traced laterally for 5 km in the area. It occurs within the homogeneous shelf mudstone of the Jagüel Formation and contains abundant volcanogenic plagioclase volcanic lithics, shell detritus and shark teeth (Palamarczuk et al., 2002). This KPg transition sandstone shows abundant rip-up clasts, erosional base, coarse-grain size, normal grading and hummocky cross-bedding, and has been interpreted as a tsunami deposit in a shelf environment, related to the Chicxulub bolide impact in Mexico (Scasso et al., 2005). Spherule, shocked quartz or enrichment of meteoritic components has not been reported from this layer or the mudstones immediately above.

Keller et al. (2007) suggest that the KPg boundary is marked by erosional-based sandstone that signifies a hiatus. This sandstone, previously interpreted as a mark of the KPg transition, contains diverse planktic foraminiferal zone P1c assemblages and nannofossils of zone NP1b immediately above (Keller et al., 2007). These authors suggested that its deposition occurred at about 500 kyr after the KPg hiatus.

4.5. Meghalaya, South Shillong Plateau, NE India

The Um Sohrynkew section is situated in northeastern India, north of Bangladesh and in a distance of about 800–1000 km from the Deccan volcanic province (Figs. 5, 6 and 7). It is exposed along the Um Sohrynkew River in Meghalaya, next to Therria village, East Khasi Hills District, south Shillong Plateau, in the eastern Himalayas (Fig. 7). The succession comprises the most complete marine KPg succession known from India, and possibly worldwide (Gertsch et al., 2011 and references therein). The section displays strong evidence of mass extinction patterns (e.g. planktic foraminifers and larger ammonoids), a preserved KPg boundary layer, as well as the first appearance of Danian foraminifers, and indications for sea-level change (Keller et al., 2008, 2009; Tewari et al., 2010a, 2010b; Gertsch et al., 2011 and references therein).

The KPg boundary at Um Sohrynkew (Fig. 5) is marked by a thin red clay layer enriched in Ir and other platinum group elements (Pandey, 1990; Bhandari et al., 1993, 1994; Garg et al., 2006) with abundant subangular quartz grains in a brown matrix (Gertsch et al. 2011). This section consists of a continuous Campanian–Eocene succession characteristic of coastal, estuarine and nearshore environments (Nagappa, 1959; Krishnan, 1968; Banerji, 1981; Tewari et al., 2010a, 2010b) with marine shelf sediments including thick sandstone layers, marl, shale and carbonates.

Based on the distribution of zonal indices, Mukhopadhyay (2008) and Pal et al. (2015) have recognized seven successive planktic foraminiferal zones across the KPg boundary at the Um Sohrynkew River section. These zones are, in stratigraphic order, CF4, CF3, CF2 and CF1 in the upper Maastrichtian part and Zone P0, Zone Pα and Subzone P1a in the lower Danian part, thus, representing a biostratigraphically continuous succession across the KPg boundary.

We focus only on 2.5 m of the Maastrichtian–Danian interval of the Um Sohrynkew section, bracketing the KPg boundary. Twenty-five samples have been stratigraphically collected at an interval of 10 cm: seven samples from greenish sandstone and greenish gray clayey marl of the Maastrichtian Mahadeo Formation, one sample from the rust-red-colored sandy–silty KPg boundary layer (about 2 cm thick) and the rest of samples from the Danian Langpar Formation whose basal portion is formed by a 10 cm-thick bioturbated sandstone overlain by dark to light gray shale to marl (Fig. 5).

4.6. Jhilmili intertrappean sediments, Madhya Pradesh, Central India

The Deccan intertrappean sediments have been regarded for long time as terrestrial deposits, Maastrichtian in age, until the work by Keller et al. (2009) who studied the sedimentology, microfacies, biostratigraphy and, C- and O-isotope chemostratigraphy of a thick intertrappean succession next to the village of Jhilmili (22°02′44″ N, 79°09′34″ E), Chhindwara District of Madhya Pradesh, central India. This succession consists of sediments with early Danian planktic foraminifera sandwiched between two basalt flow horizons (the lower and upper trap basalts correspond, respectively, to C29r and the C29r/C29n transition) (Keller et al., 2009) and is located near the main road that links Seoni and Chhindwara, exposed in a shallow-river valley. Its lithological types comprise claystones, paleosols, siltstones, clayey–silty marlstones to limestones and can be subdivided into three different units summarized below.

The 6 m thick lowermost unit (unit 1), deposited in terrestrial and palustrine environments, overlies the strongly weathered lower basalt trap. It consists of red clayey siltstone with carbonate nodules and coarser quartz grains, becoming less abundant towards the top. The unit is overlain by another about 70 cm thick lacustrine-brackish deposit (unit 2), that consists of pink, reddish to yellow laminated clays, containing marly limestones in its lower part, and with abundant volcanic glass shards. The top of this unit is formed by coarse-grained nodular limestone that was probably deposited in fresh to brackish-marine water deduced from the common freshwater and rare brackish-water ostracods along with rare planktic foraminifers (Keller et al., 2009).

Unit 3 is similar to the unit 2, consisting of red clayey siltstones, with clay and carbonate clasts interbedded with fine-sand layers. Glass spherules and shards are present as well as a carbonate-nodule layer. A 1 cm-thick black charcoal layer separates this unit from the overlying basaltic flow which is strongly weathered. Immediately below this upper basalt trap, a 30 cm-thick tempestite has been recognized.

In this intertrappean succession, Keller et al. (2009) have identified a thin aquatic interval of fresh water ponds and lakes deposits overlain by shallow coastal marine sediments with brackish marine ostracods and lower Danian zone P1a planktic foraminifers, very close to the KPg boundary. Their most important contributions were: (a) discovery of environmental changes preserved within the intertrappean sediments at Jhilmili and (b) a marine incursion pointing to the existence of a seaway at least 800 km long, across India, from the west through the Narmada–Tapti rift valley (Shukla and Srivastava, 2008; Keller et al., 2009, Fig. 6).

5. Methods

5.1. Analysis of total organic carbon (TOC), molybdenum and aluminum

All analyzed samples in this study were decarbonated using 6 M HCl prior to TOC analyses. Acid remains were subsequently

removed by a repeated procedure of rinsing, centrifugation, and decantation of supernatant liquids. Remaining fractions were weighed out again after 24 h freeze drying at temperatures of −54 °C. The $CaCO_3$ concentration was calculated by the weight difference of the aliquots before, and after the acid treatment. The total organic carbon was measured on 160 mg of decarbonated aliquot using a Carbon-Sulfur-Determinator (Eltra CS 500) at the Department of Geosciences and Natural Resources Management, University of Copenhagen. The sample was combusted for 90 s in a ceramic boat at a temperature of ~1350 °C with a catalytic oxidation process. The resulting CO_2 signal was electronically linearized and integrated, and subsequently used to calculate the TOC. The reproducibility, obtained from multiple analyses of the in-house reference material SKK-9 (TOC = 6.88%), is generally better than 0.1% (1 sd).

Molybdenum and aluminum were analyzed by ICP–MS at the Geological Survey (GEUS) in Copenhagen, Denmark after sample digestion with 6N HCl, dissolving all carbonates, but probably leaving some silicate detrital material back. These analyses are, therefore, incomplete whole-rock analyses and the reported aluminum concentrations are regarded as minimum-rock concentrations. Molybdenum has been measured over two different isotopes (^{95}Mo and ^{98}Mo) and here the total Mo concentrations are calculated from the ^{95}Mo peak.

5.2. Analysis of mercury

Mercury concentrations were determined in homogenized powdered samples at the LABOMAR in the Federal University of Ceará, Brazil, using the method described by Sial et al. (2014, p. 105) "glass and plastic ware were decontaminated by immersion for 1 day in (10% v/v) Extran solution (MERCK), followed by immersion for 2 days in diluted HCl (5% v/v) and final rinsing with Milli-Q water. All chemical reagents used were of the least analytical grade. Cold Vapor Atomic Fluorescence Spectrophotometry, using a Millenium Merlin PSA spectrophotometer, was used for Hg determination, after Hg^{2+} reduction with $SnCl_2$. All samples were analyzed in duplicates, showing reproducibility within 9.5%. A certified reference material (NIST 2702, Canada) was simultaneously analyzed to evaluate Hg determination accuracy. Such analysis showed a precision of 4%, as indicated by the relative standard deviation of three replicates, and presented Hg recovery of 98.8± 6.2%. The Hg detection limit estimated as 3 times the standard deviation of reagent blanks was 1.26 $ng \cdot g^{-1}$. In all cases, blank signals were lower than 0.5% of sample analysis. The concentration values were not corrected for recoveries found in the certified material powder, following Sial et al. (2014, p. 105)."

5.3. Analysis of carbon isotopes

Inorganic and organic $\delta^{13}C$ analyses of carbonates were performed at the Stable Isotope Laboratory (LABISE) of the Department of Geology, Federal University of Pernambuco, Brazil. Extraction of CO_2 gas was performed using a conventional high vacuum extraction line after reaction with 100% orthophosphoric acid at 25 °C for one day. Released CO_2 was analyzed in a Thermofinnigan Delta V Advantage mass spectrometer and results are reported in δ notation in permil (‰) VPDB.

$\delta^{13}C_{org}$ was analyzed from total organic carbon of insoluble residues of samples from all the studied sections. After whole-rock samples were crushed into powder "insoluble residues for organic carbon isotope analysis were obtained by acidifying these whole-rock powders in increasing concentrations (0.4, 0.6 and 0.8 mol l^{-1}) of H_3PO_4 for three days to dissolve all carbonate minerals. Care was taken to ensure that acid was added and acidification continued until there was absolutely no visible carbonate dissolution so that the analyses would not be affected by contamination from residual inorganic carbon. The insoluble residues were then rinsed with DI water, dried and loaded into tin capsules for isotopic analysis (Sial et al., 2014, p. 105)." $\delta^{13}C_{org}$ was measured using continuous flow elemental analysis isotope-ratio mass spectrometry with a Delta V Advantage mass spectrometer interfaced with a COSTECH elemental combustion system (combined analytical and sampling error of ±0.2‰).

5.4. Analysis of Hg isotopes

Mercury isotope ratios were determined on the new MC-ICP-MS (Nu-Plasma II, Nu Instruments) equipped with sixteen Faraday cups at the State Key Laboratory of Environmental Geochemistry, Institute of Geochemistry, Chinese Academy of Sciences, China, following a method similar to Huang et al. (2015). A continuous flow cold-vapor generation system (CV) was coupled with an Aridus II desolvation unit (CETAC Technologies, U.S.) for Hg and Tl introduction, respectively. The instrumental baseline was measured by de-focusing before each sample and standard. Both the internal standard method and the standard-sample bracketing technique were used to correct for instrumental mass bias (Chen et al., 2010; Jiskra et al., 2012).

Mass-dependent fractionation (MDF) of Hg isotopes is reported in delta notation, δ, which is the permil (‰) deviation relative to the SRM 3133 standard. Mass independent fractionation (MIF) of Hg isotopes is reported using upper-case delta notation, Δ, which is the deviation of the measured isotope ratio from the theoretical ratio predicted by MDF. The analytical quality was controlled by repeated measurement of standard materials. Long-term analysis gave average values of −0.54 ± 0.10‰, −0.02 ± 0.04‰ and −0.04 ± 0.04‰ for δ^{202}Hg, Δ^{199}Hg and Δ^{201}Hg of UM-Almaden Hg (2SD, n = 21), and of −1.22 ± 0.16‰, 0.06 ± 0.09‰ and 0.03 ± 0.10‰ for those of Fluka Hg (2SD, n = 13), respectively, in accordance with the published results (Bergquist and Blum, 2009; Chen et al., 2010; Chen et al., 2012; Jiskra et al., 2012). The 2SD of the isotopic compositions of the UM-Almaden were considered as the analytical uncertainty for the isotopic compositions of samples. When the uncertainty of the replicate isotopic measurements of one sample was larger than the 2SD of the UM-Almaden, the uncertainty was applied to the sample (Huang et al., 2015).

6. Results and data interpretation

6.1. Carbon-isotope chemostratigraphy and total organic carbon (TOC)

The covariation between carbonate and sedimentary organic C-isotope records can help establishing whether variations in the $\delta^{13}C_{carb}$ record reflect changes in the isotopic composition of the ancient dissolved inorganic carbon pool (e.g. Oehlert and Swart, 2014, and references therein). Covariant $\delta^{13}C_{carb}$ and $\delta^{13}C_{org}$ records evidence that both the carbonate and organic matter were originally produced in the surface waters of the ocean and have retained their original $\delta^{13}C$ composition (e.g. Korte and Kozur, 2010; Meyer et al., 2013) as it is believed that no secondary processes are able to shift $\delta^{13}C_{carb}$ and $\delta^{13}C_{org}$ in the same direction at the same rate (Knoll et al., 1986). Decoupled $\delta^{13}C_{carb}$ and $\delta^{13}C_{org}$ records indicate diagenetic alteration (e.g. Grotzinger et al., 2011; Meyer et al., 2013) or that local syn-sedimentary processes have introduced noise in the $\delta^{13}C_{org}$ record (Maloof et al., 2010).

Global $\delta^{13}C$ records of bulk sediment comparing C-isotope pathways across the KPg boundary from far apart sections at

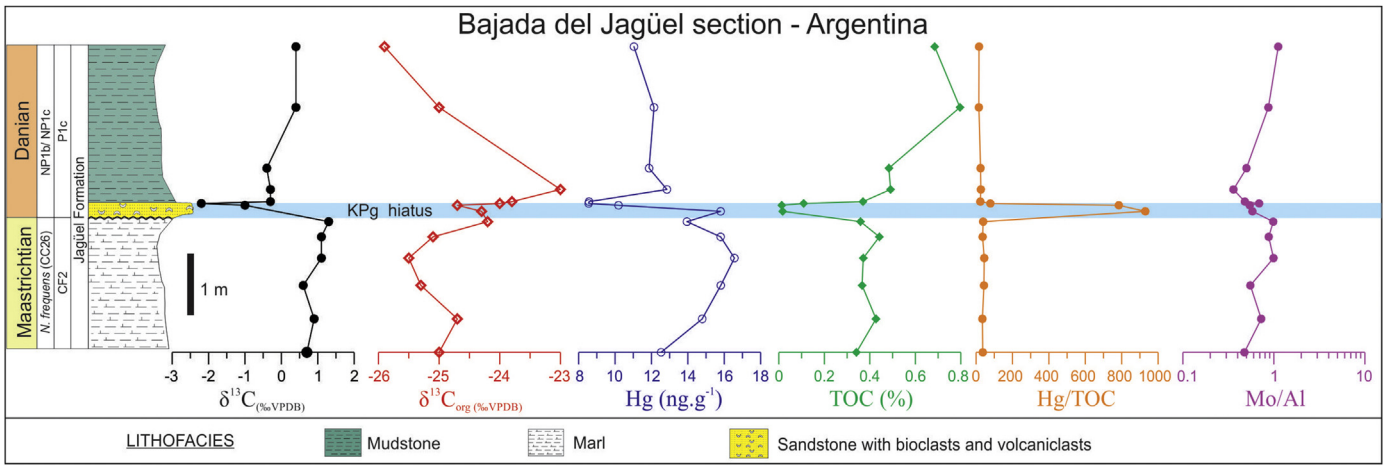

Fig. 9. $\delta^{13}C_{carb}$, $\delta^{13}C_{org}$, Hg/TOC and Mo/Al variation patterns across the KPg boundary in a section at Bajada del Jagüel, Neuquén Basin, Argentina (biostratigraphy according to Keller et al., 2007).

Højerup, Bottaccione and Bajada del Jagüel localities (Figs. 8 and 9), were previously published by Sial et al. (2014).

New $\delta^{13}C_{carb}$ data are presented here for the sections in the Meghalaya, Jhilmili and Padriciano (Tables 1 and 3; Figs. 8 and 10) and $\delta^{13}C_{org}$ for the six sections under consideration (Tables 1–3, Figs. 8, 9, 10).

Twenty-five samples were collected stratigraphically at centimeter scale, perpendicular to the strike of the strata, from a 2.5 m section across the KPg boundary at the Um Sohrynkew River in Meghalaya (Table 3; Fig. 10A). The lowermost meter in this section is composed of greenish glauconitic sandstone and greenish-gray shale belonging to the Maastrichtian Mahadeo Formation, below the yellowish brown-reddish KPg boundary clay layer (samples KT-1 through KT-7 in Table 3 lie immediately below the KPg boundary clay layer). Light to medium-gray and dark-gray to light-medium gray shale (samples KT-8 through KT-25; Table 3) were collected from the lowermost portion of the Danian Langpar Formation, immediately above the KPg boundary layer.

Twenty-four samples were collected from a 7.3 m section o intertrappean beds (Table 3; Fig. 10B) between two basaltic flow layers in a shallow river valley next to the village of Jhilmili, Chhindwara District of Madhya Pradesh. The lowermost layer in this section is composed of ferricrete paleosol with calcitic veins which is covered by a hard sediment layer within paleosol with clastic grains and calcitic cement. This is followed upward by fine-grained, brick red with yellowish tint soft ferricrete, and then by comparably harder grayish brown claystone with laminar features. Towards the top, this section contains again fine-grained, brick red soft ferricrete with yellowish tint, which is covered by a greenish clay layer with calcitic veins. Eighteen samples of carbonates from the Liburnia Formation have been collected from a representative section across the KPg boundary at a quarry at Padriciano in the Trieste Karst (Table 1; Fig. 8C).

Among the six sections in this study, the three from Europe and the one from Bajada del Jagüel display isotopically lighter carbonate composition immediately above the KPg boundary, portrayed by a shift to lighter $\delta^{13}C$ values (Figs. 8 and 9). This picture could be partially a consequence of an increase of volcanic CO_2 in the atmosphere (80% of the Deccan phase 2 eruptions took place within the time lapse recorded in the sections examined) which may have accounted also for the large negative $\delta^{13}C$ excursion at or just below the KPg boundary. Another important factor driving this negative excursion is the collapse of bioproductivity at the boundary, with a gradual recovery in the early Danian.

An abrupt decrease of $\delta^{13}C_{carb}$ at the KPg boundary is noticeable at the Højerup, Bottaccione and Meghalaya sections. At the Bajada del Jagüel and Padriciano localities, there is a strong decrease of $\delta^{13}C$ values that predate (but very close) the KPg transition. In Jhilmili, the end-Cretaceous is represented by basalt in the studied section and the $\delta^{13}C$ pathway shows a prominent minimum (−12‰) at about 1 m above the lower basaltic flow, and upsection this curve gradually shows less negative values, predominantly from −4 to −3‰.

The total organic carbon content in the studied sections, expressed as percent TOC, are <1.0% (Tables 1–3), with the majority of samples yielding values < 0.2%. Among the complete sections in this study, the highest TOC values were recorded in the KPg boundary layer in the Højerup section (~0.9%) and in the uppermost Maastrichtian and Danian portions of the Meghalaya section (0.3–0.6%), while much lower TOC values are observed in the whole Bottaccione section (0.01–0.09%). At Højerup, the TOC stratigraphic variation curve shows a very monotonous pattern with almost no oscillation except a prominent positive shift at the KPg boundary layer (Fig. 8A). At Gubbio, however, the TOC stratigraphic pathway shows vigorous oscillations with a negative shift about 4 m below the KPg boundary (within the CF2 biozone), a small negative excursion at the KPg boundary and a prominent positive shift about 8 m above the KPg boundary (within the P1a biozone). At Meghalaya, the TOC stratigraphic variation curve shows two marked positive excursions, about one meter below the KPg boundary (CF2 biozone) and another at the KPg boundary and in lowermost Danian (P0 biozone).

At the Padriciano section, the TOC values are all <0.3%, with highest values found in the Maastrichtian portion of the section and a positive shift in the KPg boundary breccia. In Bajada del Jagüel, TOC values range between 0.3 (Maastrichtian) and 0.8% (Danian), and a strong shift to values as low as 0.01% is the sandstone that marks the KPg transition (Table 2). At the Jhilmili section, the TOC stratigraphic pathway shows vigorous oscillations in the lower half of the section, followed by a strong positive shift in the upper half of this curve.

The $\delta^{13}C_{org}$ curve for organic matter from the Højerup section displays a gradual decrease of values from −23‰ towards the KPg boundary layer with a minimum of −27‰ at the KPg boundary (Fig. 8A). This is followed by a strong increase to −22‰ upsection and again by a negative shift to −27‰ and a positive shift to −22‰. At the Bottaccione section (Fig. 8B), the $\delta^{13}C_{org}$ curve shows a less pronounced decrease towards to the KPg boundary within the

CF2–CF1 biozones, a discrete decrease at the KPg boundary, and two positive shifts within the P1a biozone. The Meghalaya section shows a different pattern (Fig. 10A) with no decrease of $\delta^{13}C_{org}$ towards the KPg boundary, contrary to what was observed at Højerup and Bottaccione. At the KPg boundary, the $\delta^{13}C_{org}$ pathway shows a maximum (−21‰) within the P0 biozone, followed upsection by a monotonous variation curve within the P1a (1) subzone and a small increase to −24‰ within the P1a (2) subzone. A covariance record between $\delta^{13}C_{carb}$ and $\delta^{13}C_{org}$ at the Højerup and Bottaccione sections is depicted in Fig. 8A and B, providing evidence that the carbonate and organic matter were produced in the surface waters of the ocean and have probably retained their original respective $\delta^{13}C$ composition. At Meghalaya, the $\delta^{13}C_{carb}$ and $\delta^{13}C_{org}$ curves display opposite behaviors around the KPg boundary, with large positive excursion of the $\delta^{13}C_{org}$ curve.

The Padriciano section is characterized by a $\delta^{13}C_{org}$ curve (Fig. 8C) similar to that observed at Højerup, with a gradual decrease from −21 to −23‰ from one meter below the K–Pg transition to the KPg transition, reaching a minimum about 0.5 m above this transition, and followed upsection by a positive shift. The $\delta^{13}C_{org}$ curve for Bajada del Jagüel section exhibits a minimum (~−26‰) about 0.5 m below the KPg boundary (within the CF2 biozone), a negative excursion at the boundary, a positive excursion (−23‰) immediately above the boundary, and a gradual and strong decrease to −26‰ upsection (Fig. 9). For the Danian Jhilmili section, the $\delta^{13}C_{org}$ shows two positive shifts within the P1a biozone with a strong negative shift at the top, close to the upper basalt flow. Except for Meghalaya, the behavior of the $\delta^{13}C_{org}$ stratigraphic variation curves for these sections may possibly be explained by a response to growing deterioration of the environment at the end of the Maastrichtian with gradual decrease of organic productivity, followed by its gradual recovery early in the Danian.

6.2. Mercury concentrations, Hg/TOC and Mo/Al ratios

Mercury concentrations for stratigraphically collected samples from Højerup, Bottaccione (Table 1) and Bajada del Jagüel (Table 2) sections are available in Sial et al. (2014). The Hg variation pattern for the Højerup section displays an Hg enhancement (260 $ng \cdot g^{-1}$) that coincides with a minimum value of $\delta^{13}C$ in the Fiskeler Member at the KPg boundary (Fig. 8A). A second Hg enrichment (48 $ng \cdot g^{-1}$) is seen 1.6 m above the KPg boundary layer. In the Bottaccione section, three Hg enhancements (Fig. 8B) were observed by Sial et al. (2014), a small one (2 $ng \cdot g^{-1}$) at about 6 m below the KPg boundary, the largest one at the KPg boundary (6 $ng \cdot g^{-1}$) which coincides with a minimum of $\delta^{13}C$, and a third one at about 7 m above the KPg boundary (4 $ng \cdot g^{-1}$). In the Hg stratigraphic variation curve for the Bajada del Jagüel section (Fig. 9), three Hg enhancements are present, one at about 65 cm below the KPg boundary (17 $ng \cdot g^{-1}$ Hg), a second one at this boundary (16 $ng \cdot g^{-1}$) and a third one (13 $ng \cdot g^{-1}$) around 15 cm above that.

Hg concentrations were measured in eighteen bulk samples from Padriciano (Table 1), twenty-five from Meghalaya and eighteen from Jhilmili (Table 3) and the corresponding Hg variation patterns are shown in Figs. 8C, 10A and B. In Meghalaya, an Hg enrichment is seen at about 0.5 m below the KPg boundary layer (Fig. 10A), preceding the prominent negative $\delta^{13}C$ that marks the KPg boundary. Two prominent Hg enrichments are present in the intertrappean Danian sediments of the Jhilmili section. In the Padriciano section, the Hg stratigraphic variation pathway shows a prominent Hg enrichment (183 $ng \cdot g^{-1}$) at about 40 cm below the KPg boundary, followed by a second Hg enrichment (51 $ng \cdot g^{-1}$) at about 25 cm above the KPg boundary and a more discrete one (31 $ng \cdot g^{-1}$; Fig. 9C) at about 2.40 m above the KPg boundary.

In order to screen for Hg enrichments in these sections that represent true Hg loading to the environment, Hg concentrations have been normalized to corresponding TOC values following the approach recommended by Grasby et al. (2015a, 2015b) and Percival et al. (2015). However, in normalizing Hg concentrations to TOC, caution should be taken in using Hg-TOC pairs in which TOC concentrations are <0.2% because too low Hg concentrations may produce, in some cases, unrealistic or even false Hg/TOC spikes.

Absolute Hg concentrations, TOC, Hg/TOC and Mo/Al ratios for all the studied sections are listed in Tables 1–3 and are plotted in Figs. 8A–10B. In most cases, elevated Hg concentrations, after normalization to TOC, have generated a Hg/TOC spike. At Meghalaya, Bottaccione and Højerup, one Hg/TOC spike is observed below the KPg boundary, within the age interval of the planktic foraminiferal CF2 biozone (labeled I; Figs. 8A, B and 10A). This spike in the Bottaccione section is located about 4 m below the KPg boundary and is somewhat smaller than in the Meghalaya section. At Padriciano, a large Hg/TOC spike is observed below the KPg boundary and, perhaps, can be correlated with the spike described above, but presence of planktic foraminifers typical of the CF2–CF1 biozones has not been observed and, therefore, do not support such a correlation (Fig. 8C).

A second Hg/TOC spike is present at the KPg boundary at Højerup, Bottaccione, and Meghalaya (labeled II in Figs. 8A, B and 10A). Similar to the Hg/TOC spike I, the size of spike II is variable from place to place, being larger at Højerup. At the Padriciano section (Fig. 8C), this spike is absent as the KPg boundary is marked by an unconformity. Two large Hg/TOC spikes are present in the Jhilmili section within the planktic foraminiferal subzone P1a (labeled III and IV; Fig. 10B). At Højerup, a Hg/TOC spike is seen about 1–1.5 m above the KPg boundary (labeled III, Fig. 8A), about 4 m above the KPg boundary at Bottaccione and about 0.5 m above at Meghalaya.

At the Bajada del Jagüel section, a large Hg/TOC spike is observed in the sandstone layer that marks the unconformity at the KPg boundary (Fig. 9). The presence of volcanoclastic sedimentary grains in the sandstone is an evidence of local volcanism adjacent to the Neuquén Basin that may have contributed to enhancing the Hg/TOC ratio background prior to the KPg boundary. This positive Hg/TOC excursion may correspond to the Hg/TOC enrichment (spike II) recorded in the Højerup and Bottaccione sections. However, the paucity of the record of the CF1, Po, Pα and P1a planktic foraminiferal biozone interval, as pointed out by Keller et al. (2007), attest to a depositional or erosional hiatus of about 700 kyr bracketing the KPg boundary. Therefore, this Hg enrichment is possibly related to local volcanism next to this basin and the absence of spikes I and III could be justified by this depositional/erosional hiatus.

Covariation between Hg and Al_2O_3 (mostly associated with clays) is observed in some sections across the KPg boundary and this led to the suggestion that Hg was probably adsorbed onto continental clays with subsequent transport and deposition into the sea (e.g. Sial et al., 2013). However, there is no clear correlation between Al_2O_3 and Hg/TOC (Tables 1–3), except in the KPg boundary layer at Højerup (Fiskeler Member).

Molybdenum in sedimentary rocks has been suggested as an important elemental proxy for anoxia (e.g. Bond et al., 2015; Grasby et al., 2015a). Based on results from the Cariaco Basin, north central coast of Venezuela, Lyons et al. (2003) demonstrated a high correlation between TOC content and Mo/Al ratio in euxinic sediments and, therefore, Mo/Al trends may allow calculating the TOC composition. According to Wilde et al. (2004), however, this method demands refinement and no universal elemental proxy for determining TOC has been established so far. Mo/Al ratios are useful for discerning the original compositions of ancient rocks that were subjected to later diagenetic, low-grade metamorphism or weathering.

Table 1
C and O isotopes (‰ VPDB), total organic carbon (TOC %) and Hg ($ng \cdot g^{-1}$) across the KPg boundary in sections at Højerup (Denmark), and Bottaccione and Padriciano (Italy).

(a) Højerup section, Stevns Klint, Denmark

Formation	Member	Sample	Height (cm)	$\delta^{13}C$ ‰ VPDB	$\delta^{13}C_{org}$ ‰ VPDB	Hg ($ng \cdot g^{-1}$)	TOC(%)	Hg/TOC	Mo (ppm)	Al (%)	Mo/Al
Danian	Korsnæb Member	SKc	1050	1.4	–	1.8	–	–	–	–	–
Stevns Klint Formation		N7	990	1.19	−20.85	1.0	0.010	100.0	0.06	0.02	3.00
		N6	960	1.38	−25.76	48.2	0.029	1662.06	0.11	0.07	1.57
		N5	930	1.28	−26.82	6.8	0.020	340.00	0.08	0.02	4.00
		N4	900	1.23	−21.68	11.7	0.013	900.00	0.11	0.03	3.66
		N3	870	1.16	−21.57	3.0	0.044	68.18	0.23	0.03	7.66
		N2	840	1.28	–	6.6	0.030	220.00	0.15	0.04	3.75
Danian	Cerithium Limestone Member	D3	830	1.4	–	4.55	–	–	–	–	–
Rødvig Formation		D2	815	1.6	–	4.51	–	–	–	–	–
		N1	810	1.15	−24.94	4.5	0.006	750.00	0.15	0.04	3.75
		No. 3	805	1.7	–	2	0.030	66.66	0.14	0.06	2.33
	Fiskeler Member (KPg boundary)	FC-1	804	–	–	127.72	0.859	148.68	1.83	1.14	1.60
		FCD	803	1.9	−25.36	67.9	0.944	71.92	3.67	2.28	1.60
		FCC	802	1.7	−26.52	257.94	0.859	300.27	3.67	2.28	1.60
		FCB	801	1.3	–	194.53	0.944	206.06	3.67	2.28	1.60
		FCA	800	1.3	–	108.76	0.944	115.21	3.67	2.28	1.60
Maastrichtian	Højerup Member (gray chalk)	M2	785	1.8	–	9.09	–	–	–	–	–
Møns Klint Formation		N (−1)	770	0.71	−24.94	–	0.014	–	0.02	0.01	2.00
		M1A	770	1.7	–	0.88	0.014	62.85	0.02	0.01	2.00
		No. 2	760	1.8	–	2.3	–	–	–	–	–
		N (−2)	740	1.71	−24.20	<1.26	0.041	30.73	0.08	0.01	8.00
		N (−3)	685	1.94	−23.03	4.6	–	–	–	–	–
		N (−4)	660	1.93	−22.80	6.5	0.015	433.3	0.01	0.01	1.00
	Sigerslev Member (white chalk)	No. 1	0	1.7	–	11.3	–	–	–	–	–

(b) Bottaccione section, Italy

Lithology	Sample	Height (cm)	$\delta^{13}C_{carb}$ ‰ VPDB	$\delta^{13}C_{org}$ ‰ VPDB	Hg ($ng \cdot g^{-1}$)	TOC (%)	Hg/TOC	Mo (ppm)	Al (%)	Mo/Al
Marl	GP-28	1685.4	1.26	−25.32	3.44	0.064	53.75	0.19	0.32	0.59
	GP-27	1565.4	1.27	−24.82	1.62	0.066	24.54	0.15	0.31	0.48
	GP-26	1495.4	1.38	−20.97	3.79	0.094	40.31	0.16	0.41	0.39
	GP-25	1395.4	1.18	−27.34	1.51	0.064	23.59	0.18	0.31	0.58
	GP-24	1295.4	1.43	−27.97	1.55	0.039	39.74	0.19	0.22	0.86
	GP-23	1195.4	1.34	−26.96	1.83	0.030	61.00	0.17	0.25	0.68
	GP-22	1095.4	1.28	−28.21	0.87	0.042	20.71	0.24	0.39	0.61
	GP-21	995.4	1.48	−25.49	0.42	0.022	19.09	0.15	0.20	0.75
	GP-20	895.4	1.58	−25.02	0.68	0.045	15.11	0.21	0.30	0.70
Marl (rhytmites; carbonate production decreases in the Danian)	GP-19	875.4	1.77	−27.25	0.57	0.033	17.27	0.34	0.57	0.91
	GP-18	845.4	2.02	–	0.72	0.035	20.57	0.39	0.32	1.21
	GP-17	815.4	2.08	–	0.44	0.023	19.13	0.12	0.15	0.80
	GP-16	795.4	2.03	−24.39	0.75	0.044	17.04	0.21	0.17	1.23
Greenish brown clay layer	GP-15	(KPg boundary layer) −26.78			5.23	0.027	193.70	0.49	0.64	0.29
Mudstone with planktic foraminifera	GP-14	794	2.28	−25.36	0.22	0.018	12.22	0.09	0.37	2.67
	GP-13	790	2.32	−24.24	0.16	–	–	0.07	0.26	0.26
	GP-12	780	2.29	−25.55	0.35	0.026	13.46	0.08	0.25	0.32
	GP-11	770	2.27	−25.35	0.22	0.059	3.72	0.05	0.30	0.16
	GP-10	760	2.24	−25.55	0.37	0.041	9.02	0.06	0.21	0.28
	GP-9	730	2.17	–	0.38	0.045	8.44	0.20	0.34	0.58
	GP-8	700	2.18	–	0.47	0.049	9.59	0.17	0.26	0.65
	GP-7	600	2.07	−25.19	0.42	0.027	15.55	0.23	0.39	0.58
	GP-6	500	2.15	–	0.88	0.068	12.94	0.17	0.23	0.73
	GP-5	400	2.32	−24.83	0.48	0.017	28.23	0.30	0.59	0.50
	GP-4	300	2.13	−23.32	0.97	0.015	64.66	0.23	0.43	0.53
	GP-3	200	2.15	−27.13	1.38	0.036	38.33	0.18	0.37	0.48
	GP-2	100	2.23	−27.18	1.75	0.033	53.03	0.58	0.57	1.01
	GP-1	0	2.29	−25.11	0.37	0.091	4.06	0.26	0.78	0.33

(c) Padriciano section, Italy

Stage	Formation	Sample	Height (m)	$\delta^{13}C$ ‰ VPDB	$\delta^{13}Corg$ ‰ VPDB	Hg $ng \cdot g^{-1}$	TOC (%)	Hg/TOC	Mo (ppm)	Al (%)	Mo/Al
Danian	Liburnia	VT 16	6.4	−8.0	−22.86	6.8	0.164	41.46	1.82	0.01	182
		VT 15	5.9	−9.5	–	2.9	–	–	1.08	0.01	108
		VT 14	5.2	−9.1	−22.09	17.5	0.104	168.26	3.33	0.08	41.62
		VT 13	4.5	−9.8	−19.32	31.1	0.097	320.61	4.89	0.02	244.50
		VT 12	4	−9.6	−21.03	15.2	–	–	2.97	0.01	297
		VT 11	3.8	−9.6	–	8.6	0.161	53.41	5.36	0.01	536
		VT 10	3.65	−9.4	–	33.6	–	–	–	–	–
		VT 9	3.15	−8.5	–	41.2	–	–	–	–	–
		VT 8	2.75	−8.2	−25.20	49.9	0.169	295.26	1.96	0.02	98.00
		VT 7	2.55	−8.8	–	15.9	0.168	94.64	1.96	0.01	196
		VT 6	2.35	−8.5	–	50.5	–	–	–	–	–
		VT 5	2.15	−8.8	−22.37	12.0	0.063	190.47	11.79	0.01	1179.00

(*continued on next page*)

Table 1 (*continued*)

(c) Padriciano section, Italy

Stage	Formation	Sample	Height (m)	$\delta^{13}C$ ‰ VPDB	$\delta^{13}Corg$ ‰ VPDB	Hg ng·g^{-1}	TOC (%)	Hg/TOC	Mo (ppm)	Al (%)	Mo/Al
KPg boundary		KPg breccia	2.1	−8.5	–	16.8	0.203	82.75	1.47	0.01	147
Maastrichtian		VT 4	1.8	−8.4	−21.32	67.3	0.103	653.39	8.52	0.02	426.00
		VT 3	1.4	−7.6	–	182.5	0.181	1008.28	25.16	0.04	629.00
		VT 2	0.7	−8.7	−20.18	16.7	0.298	56.04	0.88	0.01	88
		VT 1	0.25	−3.7	−21.05	6.9	0.283	24.38	1.17	0.00	0
		VT 0	0	−3.8	−20.51	5.9	0.225	26.22	8.76	0.01	876

Molybdenum concentrations, analyzed in almost all samples in this study, have been normalized to corresponding Al values (Figs. 8A–10B). At Højerup, low values of Mo/Al ratio characterize the topmost Maastrichtian (0.50 cm below the KPg boundary) and no correlation is observed between this ratio and TOC. Within the Fiskeler Member clays, Mo/Al ratios are enhanced, while $\delta^{13}C_{org}$ changes to higher values and a positive shift of TOC values is observed. In the Cerithium Limestone and Stevns Klint Formation, in the lower Danian, no correlation between TOC and Mo/Al is apparent and Mo/Al ratios are higher than in the Fiskeler Member.

At Bottaccione, Mo/Al ratios are low, with a monotonous stratigraphic variation curve in the upper Maastrichtian, but a negative shift is seen about 0.50 cm below the KPg boundary, coinciding with vigorous positive-negative shifts in TOC values followed by a positive one of Mo/Al at the KPg boundary. At Meghalaya, Mo/Al ratios are low in the upper Maastrichtian, but likewise Højerup and Bottaccione, it shifts to lower values within 20 cm below the KPg boundary, opposite to TOC values which exhibit higher values. In the Bajada del Jagüel section, Mo/Al ratios are also low, but with little variation and no particular correlation with TOC is apparent. In the Danian Jhilmili section, Mo/Al ratios are low, and in the lower half of this section no correlation is seen with TOC but in the upper half of the section there is a weak correlation with TOC values. In the Bottaccione, Padriciano, Meghalaya, and Bajada del Jagüel sections, minimum Mo/Al ratios do not coincide with $\delta^{13}C_{org}$ peaks. The Højerup section is the only one which departs from this rule.

Lowrie et al. (1990) investigated the origin of the whitish limestone beds at about 20–50 cm below the KPg boundary in the Bottaccione and Contessa sections at Gubbio. They believed that these white beds were deposited under the same conditions as the underlying pink beds of the Scaglia Rosa Formation whose whitening is related to removal of Fe^{2+} ions by downward infiltration of reducing waters resulting from large quantity of organic matter produced by the extinction at the KPg boundary. However, Abrajevitch et al. (2015) demonstrated that a process of downward percolation of organic-rich fluids is unlikely at Bidart and Gubbio and the stratigraphic record of Mo/Al redox proxy in the studied KPg sections here suggests that Hg/TOC spikes are likely not related to decrease in oxygenation. Therefore, anoxia was not the main cause for anomalous Hg/TOC observed across the KPg boundary.

6.3. Hg isotopes

Mercury isotope analyses for the Hg spikes in the complete Højerup (Fiskeler Member), Bottaccione (Scaglia Rossa Formation) and Meghalaya sections, besides Jhilmili, Padriciano and Bajada del Jagüel sections are listed in Table 4, with results reported in delta notation in permil (‰) relative to NIST SRM 3133 Hg standard. Six analyses from a section at Bidart, part of the Basque basin, France, one of the most complete KPg boundary successions known (Bonté et al., 1984; Galbrun and Gardin, 2004; Font et al., 2014, 2016), were included for comparison and are plotted alongside the analyses for all sections in this study in Fig. 11. In this Figure, $\delta^{202}Hg$ (MDF) for all analyzed samples were plotted against corresponding $\Delta^{201}Hg$ (MIF) values and the ranges for volcanic emission and chondrite/volcanic emission Hg are indicated.

Two samples from the Meghalaya section yielded $\delta^{202}Hg$ values of −1.61‰ (spike I) and −1.89‰ (spike II) and $\Delta^{201}Hg$ close to 0.0‰. Three among four of the analyzed samples (spike II) from the Fiskeler Member at Højerup yielded $\delta^{202}Hg$ between −1.00 and −2.00‰ and two of them display positive $\Delta^{201}Hg$ or negative but very close to 0.0‰. One sample from the KPg boundary layer at the Bottaccione section in Gubbio (Spike II) yielded a $\delta^{202}Hg$ value of −1.28‰ and positive $\Delta^{201}Hg$. In addition, Hg isotopes were analyzed in six samples from Bidart which yielded $\delta^{202}Hg$ values from −0.25 to −2.66 and all positive $\Delta^{201}Hg$ values (Fig. 11). A sample from the KPg boundary layer from which Font et al. (2016) determined a true Hg spike (corresponding to spike II in this study) yielded a $\delta^{202}Hg$ value of −0.74 compatible with volcanic or chondrite source Hg. So, in the light of or current Hg isotope data, a volcanic source for Hg in the KPg boundary (spike II) is likely at these classical KPg localities.

One sample from the Padriciano locality (spike I) yielded a $\delta^{202}Hg$ value of −1.38‰ and slightly positive $\Delta^{201}Hg$, and as in Meghalaya, Hg isotopes seem to support volcanic source for the spike I in these two localities. One sample from spike III at the Jhilmili site showed a value of −1.01‰ and negative $\Delta^{201}Hg$ while another sample (spike labeled IV) yielded a $\delta^{202}Hg$ value of −2.18‰ and a $\Delta^{201}Hg$ value of −0.28‰. While the Hg isotope signature for spike III seems to support a volcanic origin, the one for spike IV suggests some post-depositional alteration. Among the twelve samples from Jagüel Formation, nine show $\delta^{202}Hg$ between −1.00 and −2.00‰ and $\Delta^{201}Hg$ are all positive, compatible with a volcanic source Hg.

Interestingly, most of the analyzed samples in this study show slightly, but significantly higher than the analytical precision of 0.04‰, positive $\Delta^{201}Hg$ signatures. Since most continental samples (soils, sediments and land plants) usually display negative or close to zero $\Delta^{201}Hg$, and post-deposition and diagenetic processes likely would not induce odd-MIF, the positive $\Delta^{201}Hg$ values observed in most samples here indicate a long-term atmospheric transport prior to deposition. During transportation in the atmosphere, photoreduction of gaseous oxidized Hg (GOM) would enrich odd isotopes in water droplets and particles, for example by adsorption, thus triggering positive $\Delta^{201}Hg$ values in final deposition (Chen et al., 2012; Blum et al., 2014). Our results seem point to Hg isotopes as a promising way for identification of the Hg source.

7. Discussion

From the Hg/TOC stratigraphic patterns in this study, one is tempted to outline a preliminary picture of the global Hg loading to the environment during the 750 kyr of Deccan phase-2 volcanic eruptions. However, as organic matter content in the examined sections tend to be very low (<0.2%), reliable Hg/TOC ratios are not always obtained and so these ratios should be looked with caution.

Table 2
C- and O-isotope analyses (‰ VPDB), total organic carbon (TOC, %), Hg (ng·g^{-1}), Mo (ppm) and Al (%) in a KPg section at Bajada del Jagüel, Argentina.

(a) Bajada del Jagüel section, Neuquén Basin, Argentina

Formation	Lithology	Sample	Height (m)	$\delta^{13}C_{‰\ VPDB}$	$\delta^{13}C_{org\ ‰\ VPDB}$	Hg (ng·g^{-1})	TOC (%)	Hg/TOC	Mo (ppm)	Al (%)	Mo/Al
Jagüel Formation	Mudstone	KT 12	5.03	0.4	−25.9	11.04	0.685	16.11	1.92	1.72	1.11
		KT 11	4.03	0.4	−25.0	12.14	0.796	15.25	1.07	1.23	0.86
		KT10	3.03	−0.4	–	11.87	0.484	24.52	0.78	1.56	0.50
		KT9	2.68	−0.3	−23.0	12.85	0.491	26.17	0.55	1.53	0.35
		KT 8	2.48	−0.3	−23.8	8.57	0.370	23.16	0.61	1.27	0.48
	Sandstone with	KT7	2.45	−2.2	−24.0	8.55	0.109	78.44	0.75	1.09	0.68
	bioclasts and volcaniclasts	KT 6	2.42	−1	−24.7	10.19	0.013	783.84	0.57	1.05	0.54
		KT 5	2.32	−0.6	−24.3	15.80	0.017	929.41	0.75	1.29	0.58
	Marl	KT 4	2.15	1.3	−24.2	13.95	0.359	38.85	1.17	1.19	0.98
		KT 3	1.9	1.1	−25.1	15.8	0.442	35.74	1.36	1.55	0.87
		KT 2	1.55	1.1	−25.5	16.56	0.371	44.63	1.09	1.10	0.99
		KT 1	1.1	0.6	−25.3	15.81	0.366	43.19	0.59	1.07	0.55
		KT0	0.55	0.9	−24.7	14.79	0.427	34.63	0.74	1.02	0.72
		KT (-1)	0	0.7	−25.0	12.53	0.341	36.74	0.56	1.18	0.47

Table 3
C- and O-isotope analyses (‰ VPDB, %), total organic carbon (TOC, %), and Hg (ng·g^{-1}) in samples from India.

(a) Meghalaya section, Um Sohrynkew, northeastern India.

Formation	Lithology	Sample	Height (cm)	$\delta^{13}C\ ‰\ _{VPDB}$	$\delta^{13}C_{org}\ ‰\ _{VPDB}$	Hg ng·g^{-1}	TOC (%)	Hg/TOC	Mo (ppm)	Al (%)	Mo/Al
Langpar (Danian)	Light gray shale	KT 25	10	0.1	−23.78	10.3	0.042	245.23	–	–	–
	Dark gray shale	KT 24	10	1.1	−25.36	9.8	0.039	251.28	–	–	–
		KT 23	10	0.4	−24.96	7.4	0.040	185.00	–	–	–
		KT 22	10	0.6	−24.35	11.5	0.039	294.87	–	–	–
		KT 21	10	−0.1	−24.93	2.4	0.042	57.14	–	–	–
		KT 20	10	0.4	−24.91	7.8	0.036	216.66	–	–	–
		KT 19	10	−0.1	−24.42	3.9	0.044	88.63	–	–	
		KT 18	10	−0.1	−24.43	12.1	0.041	295.12	–	–	–
		KT 17	10	0.6	−24.38	6.2	0.065	95.38	–	–	–
		KT 16	10	1.3	−24.59	6.7	0.039	171.79	–	–	–
		KT 15	10	1.4	−24.79	10.0	0.035	285.71	–	–	–
		KT 14	10	1.1	−24.77	11.8	0.033	357.57	–	–	–
		KT 13	10	−0.0	−24.49	4.3	0.039	110.25	–	–	–
		KT 12	10	−0.1	−24.56	1.6	0.627	2.55	2.05	1.13	1.81
	Light gray shale	KT 11	10	0.1	−21.69	2.8	0.571	4.90	2.93	1.05	2.79
		KT 10	10	0.1	−21.99	0.0	0.447	0.00	0.71	1.39	0.51
		KT 9	10	0.5	−20.22	0.0	0.468	0.00	0.53	1.16	0.45
KPg boundary layer	Yellowish brown to reddish layer	KPg bulk	10	−8.13	−23.12	6.3	0.059	16.94	3.11	1.81	1.71
Mahadeo (Maastrichtian)	Greenish sandstone	KT8	10	−0.4	−23.93	6.3	–	–	–	–	–
	and shale	KT7	10	0.4	−23.91	3.2	–	–	–	–	–
		KT6	10	−0.0	−23.91	6.2	0.070	88.57	0.66	1.50	0.44
		KT5	10	0.7	−24.14	2.9	0.052	55.76	0.59	1.45	0.40
		KT4	10	0.2	−24.82	13.1	0.335	39.10	1.67	1.22	1.36
		KT3	10	0.5	−23.81	98.6	0.424	232.54	1.21	1.53	0.79
		KT2	10	0.3	−24.49	31.4	0.337	93.17	1.88	1.18	1.59
		KT1	10	1.0	−24.54	6.9	0.349	19.77	0.91	1.12	0.81

(b) Jhilmili Section, central India

	Lithology	Sample	Height (m)	$\delta^{13}C\ ‰\ _{VPDB}$	$\delta^{13}C_{org}\ ‰\ _{VPDB}$	Hg ng·g^{-1}	TOC (%)	Hg/TOC	Mo (ppm)	Al (%)	Mo/Al
Upper Basalt Trap	2.5 m thick basaltic flow	JMR 20	0.5	–	−20.73	12.4	0.030	413.33	0.13	2.14	0.060
Paleosol Section (Danian)	Greenish clay layer with	JMR 19	0.3	−3.7	−28.27	15.3	0.093	164.51	0.07	1.97	0.035
	calcitic veins	JMR 18	0.5	−5.6	−25.44	12.3	0.060	205.00	0.04	1.74	0.022
	Soft ferricrete fine-grained,	JMR 17	0.5	−3.3	−20.73	8.7	0.041	212.19	0.03	3.73	0.008
	brick red with yellowish tint	JMR 16	0.5	−2.6	−23.33	100.2	0.032	3131.25	0.01	2.29	0.004
		JMR 15	0.5	−2.6	–	19.2	0.036	533.33	0.01	2.21	0.004
		JMR 14	0.5	−3.20	−24.45	9.9	0.024	412.50	0.03	2.22	0.013
	Claystone with laminar features,	JMR 13	0.3	−3.5	−25.53	17.7	0.067	264.17	0.07	2.29	0.030
	grayish brown in color,	JMR 12	0.4	−3.3	−24.92	6.2	0.045	137.77	0.64	2.62	0.244
	relatively harder	JMR 11	0.6	−4.7	−23.26	14.8	0.078	189.74	1.68	1.65	1.018
	Soft ferricrete, fine- grained,	JMR 10	0.3	−4.1	–	51.8	0.039	1328.20	0.36	3.07	0.117
	brick red with yellowish tint	JMR 09	0.3	−6.0	−23.38	14.5	0.035	414.28	0.82	2.49	0.329
		JMR 08	0.3	−8.0	−25.31	11.8	0.056	210.71	0.07	3.94	0.017
		JMR 07	0.5	–	−20.33	19.0	0.062	306.45	0.05	3.79	0.013
	Hard sediment layer within the	JMR 06	0.3	−11.0	−24.68	14.5	0.053	273.58	0.60	2.03	0.295
	paleosol with clasitc grains with calcitic cement	JMR 05	0.5	−12.1	−24.41	24.1	0.074	325.67	0.04	3.56	0.011
	Lowest layer of paleosol ferricrete	JMR 04	0.5	−3.4	−24.43	20.7	0.046	450.00	0.28	2.71	0.103
	with calcitic veins	JMR 03	0.5	−9.9	−22.97	11.8	0.084	140.47	0.03	3.88	0.007
Lower Basalt Trap	2.0 m thick basaltic flow	JMR 02	0	–	–	–	0.071	–	0.04	1.48	0.027

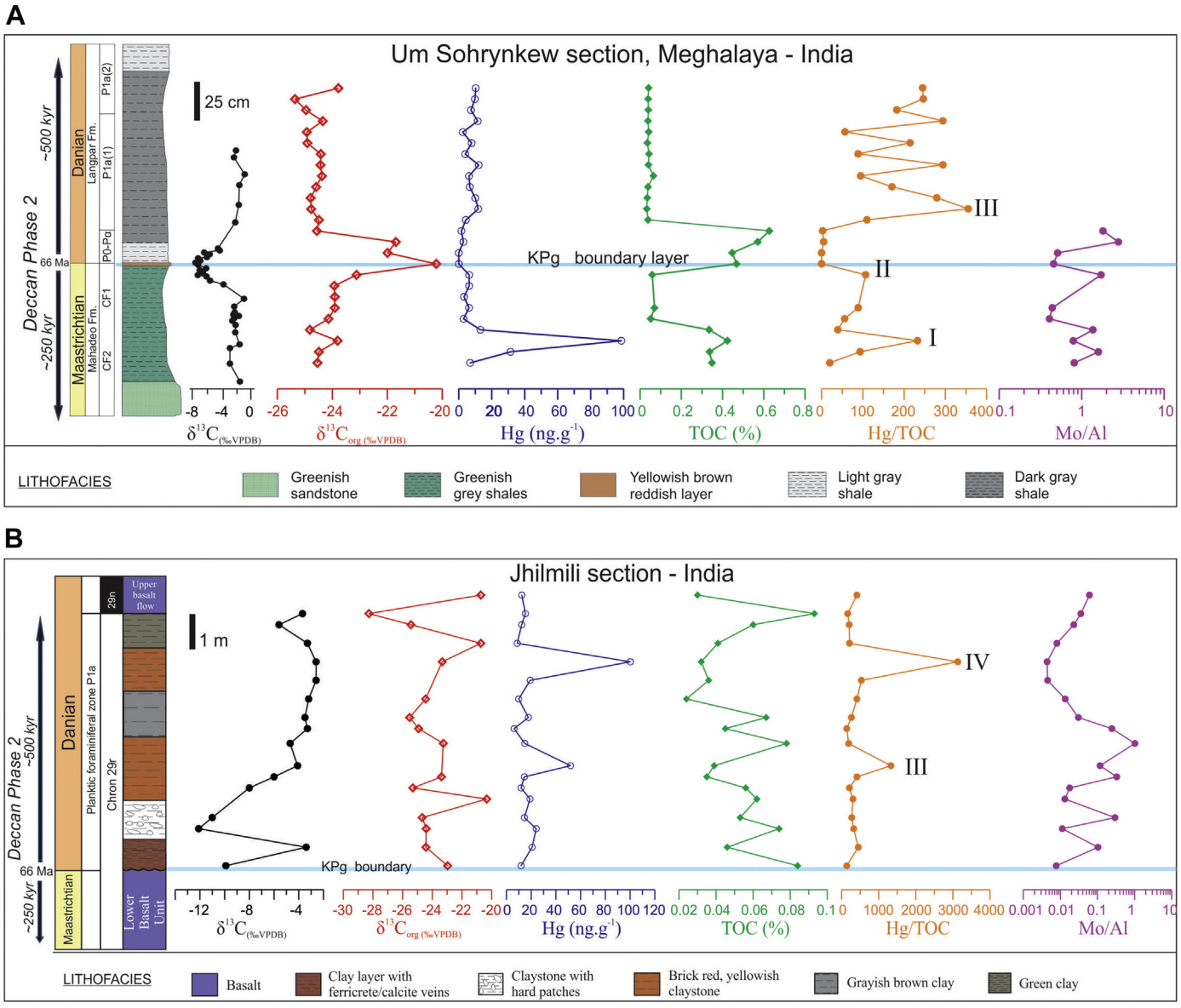

Fig. 10. $\delta^{13}C_{carb}$, $\delta^{13}C_{org}$, Hg/TOC and Mo/Al variation patterns across the KPg boundary at: (A) Um Sohrynkew River section (Meghalaya), south Shillong Plateau, northeastern India ($\delta^{13}C_{carb}$ from Gertsch et al., 2011; planktic foraminifera biostratigraphy from Mukhopadhyay, 2008; Pal et al., 2015) and (B) Jhilmili section, Madhya Pradesh, central India (planktic foraminiferal biostratigraphy from Keller et al., 2009).

Three Hg/TOC spikes are depicted from the three examined complete sections. One of them observed within the CF2 foraminiferal biozone in Meghalaya, Højerup and Bottaccione sections (spike-I), in agreement with increased Hg loading to the atmosphere by early stages of Deccan phase-2 eruptions, between 250 and 160 Kyr before the KPg boundary. Too low TOC values at Højerup and Bottaccione resulted at enrichment of the Hg spike I in these two sections. As there is no foraminifer biozone control at Padriciano, we speculate that the prominent Hg enrichment observed at this section (182 ng·g^{-1} of Hg), about one meter below the KPg boundary, is coeval with the spike-I in the Meghalaya section. An apparent Hg spike (16 ng·g^{-1}) at about one meter below the KPg boundary at Bajada del Jagüel, recognized by Sial et al. (2014), disappears after TOC normalization.

It became evident from this study that a second Hg/TOC spike (spike-II) coincides with the KPg boundary layer at Højerup and Bottaccione. At Meghalaya, presence of an Hg enhancement in the proximity of the KPg boundary becomes evident only after normalization of the Hg concentration to TOC. In this case, a proximal section to the Deccan, the Hg loading was only detected after normalization to TOC. Enrichment of Hg in the KPg boundary at Padriciano, if any, was probably swept off by erosion that preceded deposition of the breccia that marks this boundary. It is uncertain whether the notable Hg/TOC spike in the KPg boundary at Bajada del Jagüel is correlated to spike II or resulted from Hg loading from local volcanism within the Neuquén Basin. A third Hg/TOC spike in the Danian (spike III) at Jhilmili, a very proximal section at the Deccan volcanic center, Højerup, Bottaccione and Meghalaya within the P1a foraminiferal biozone, seems to be a record of late stages of Deccan phase-2 eruptions within the 220–500 kyr after the KPg boundary.

Around 66 Ma ago, the Højerup and Bottaccione sites were located at similar distances relative to both the Deccan Traps and the Chicxulub impact site (Fig. 1), therefore similar-sized Hg peaks would be expected. “Two explanations for the observed discrepancy may be offered: (a) divergence in time lengths and/or factors

Table 4
Hg isotopes (‰ relative to NIST SRM 3133) in samples with Hg enrichments: spike I (Meghalaya, Padriciano); spike II (Højerup, Bottaccione, Meghalaya), and Bidart (France; for comparison); spike III (Jhilmili), besides samples from across the KPg boundary at Bajada del Jagüel.

Samples	δ^{199}Hg	δ^{200}Hg	δ^{201}Hg	δ^{202}Hg	Δ^{199}Hg	Δ^{200}Hg	Δ^{201}Hg
Mass dependent fractionation (MDF)					Mass independent fractionation (MIF)		
(a) Fiskeler Member (KPg boundary layer), Denmark							
FCA	−0.51	−1.06	−1.76	−2.34	0.08	0.11	−0.01
FCB	−0.28	−0.74	−1.18	−1.62	0.13	0.07	0.04
FCC	−0.29	−0.55	−0.86	−1.06	−0.02	−0.02	−0.06
FCD	−0.43	−0.92	−1.44	−1.93	0.06	0.05	0.01
(b) Bottaccione, Italy (KPg boundary layer)							
GP-15	−0.26	−0.59	−0.93	−1.28	0.06	0.05	0.03
(c) Meghalaya, India							
KT-3	−0.35	−0.78	−1.16	−1.61	0.06	0.03	0.05
KT-bulk	−0.64	−0.94	−1.58	−1.89	−0.16	0.01	−0.16
(d) Jhilmili, India							
JM-16	−0.60	−0.57	−0.98	−1.01	−0.34	−0.06	−0.22
JM-10	−1.01	−1.12	−1.92	−2.18	−0.46	−0.02	−0.28
(e) Padriciano, Italy							
VT-3	−0.08	−0.69	−1.00	−1.38	0.27	0.00	0.04
(f) Jagüel Formation, Neuquén Basin, Argentina							
K-T-12	0.07	−0.29	−0.29	−0.62	0.22	0.02	0.18
K-T-11	−0.08	−0.67	−0.89	−1.41	0.27	0.04	0.17
K-T-10	−0.14	−0.59	−0.77	−1.17	0.16	−0.01	0.10
K-T-9	−0.13	−0.59	−0.76	−1.18	0.17	0.00	0.13
K-T-8	−0.06	−0.59	−0.74	−1.15	0.13	−0.01	0.12
K-T-7	−0.08	−0.52	−0.68	−1.00	0.17	−0.02	0.08
K-T-6	−0.10	−0.48	−0.61	−0.87	0.12	−0.05	0.04
K-T-5 (KPg layer)	−0.14	−0.57	−0.73	−1.05	0.13	−0.05	0.06
K-T-4	−0.03	−0.36	−0.49	−0.77	0.17	0.02	0.09
K-T-3	−0.12	−0.60	−0.88	−1.27	0.20	0.04	0.07
K-T-2	−016	−0.61	−0.84	−1.22	0.15	0.01	0.08
K-T-1	−0.12	−0.50	−0.68	−1.04	0.14	0.02	0.10
(g) Bidart, France							
KPg boundary layer	−0.04	−0.34	−0.42	−0.74	−1.12	−0.15	0.03
BI-9.28.5	−0.11	−0.57	−0.66	−1.44	−1.56	0.25	0.15
BI-9.34.2	0.05	−0.11	−0.13	−0.31	−0.73	0.12	0.04
BI-9.36.2	0.08	−0.10	−0.07	−0.25	−0.61	0.15	0.03
BI-10.35.1	−0.33	−1.28	−1.68	−2.66	−4.30	0.33	0.06
BI-11.7.3	0.13	−0.16	−0.04	−0.66	−0.73	0.30	0.17

governing Hg deposition, (b) preservation of Hg deposit from weathering and diagenesis. The high level of Hg recorded at the KPg boundary layer at Højerup may have resulted from an increased flux of volcanic-derived Hg from the landmass into the marine realm. At Bottaccione, Hg accumulation likely resulted from a similar mechanism, but a distal, deep marine (pelagic) setting probably determined a lower Hg concentration if compared to the more proximal Højerup section. However, as the KPg boundary layer has been tectonically tilted at Bottaccione, this could have also facilitated a gradual Hg leaching, resulting in a more modest remaining Hg enrichment" (Sial et al., 2014, p. 111–112). One cannot discard the possibility of acid rain leaching of Hg in the aftermath of the KPg boundary event. It is difficult to estimate how much mountain chains, dispersion corridors along latitudinal zones, winds and marine currents have affected the Hg transport and deposition during the KPg transition. Due to climate changes, the environment at that time was probably depleted of organic scavenging capacity and, therefore, Hg^{+2} was likely kept in solution, readily adsorbed onto clays and transported to the sea/ocean.

Large differences in Hg peak magnitude, as observed between Højerup and Bottaccione, are also observed in sections bracketing the KPg boundary within a single basin (e.g. Salta and Neuquén basins; Sial et al., 2013, 2014). One cannot totally discard the possibility that the Chicxulub asteroid impactor may have carried a large amount of Hg. If Hg concentrations measured in the CI-chondrite Orgueil were typical for the KPg boundary asteroid impactor, full release of highly volatile Hg would correspond to a total injected mass of 10^6–10^7 metric tons of Hg according to Meier et al. (2015), that is, 10^4–10^5 times higher than present annual anthropogenic emissions, implying a global Hg deposit of several thousand ng Hg/cm^2. Small Hg peaks recorded at the KPg boundary have been attributed to terrestrial response to the Chicxulub impact by Hildebrand and Boynton (1989) or to volcanic activity pulses (Sial et al., 2013, 2014; Font et al., 2016). Meier et al. (2015) measured the concentration and isotopic composition of Hg in meteorites and at some KPg boundary sites, including Højerup, Bidart (France) and Teapot Dome sites (USA). At Teapot Dome, they found a huge, double-spiked Hg peak of ~1000 ng·g^{-1}, and much smaller Hg concentrations at Højerup (200 ng·g^{-1}) and Bidart (80 ng·g^{-1}). The Hg isotopic composition in Hg spikes in sedimentary rocks spanning the KPg boundary can potentially help constraining the Hg source. Meier et al. (2015) did not report Hg isotope compositions measured in their study of meteorites and KPg boundary sites to allow further comparison with the Hg isotope data reported in the present study.

The δ^{202}Hg data in clays from the KPg boundary layer at Højerup, from the KPg boundary clay layer in the Scaglia Rossa Formation at Bottaccione and from Meghalaya (spike II) besides from Hg in the spike I (Meghalaya and Padriciano) and spike III at Jhilmili lie within the range for volcanogenic Hg (0.00 to −2.00‰) as reported by Bergquist and Blum (2009). The small and positive Δ^{201}Hg (Table 4) also sheds light on the long-range atmospheric transport of volcanic emission.

8. Conclusions

(a) Three Hg/TOC spikes present in the studied complete sections (Meghalaya, Højerup and Bottaccione) are proposed to

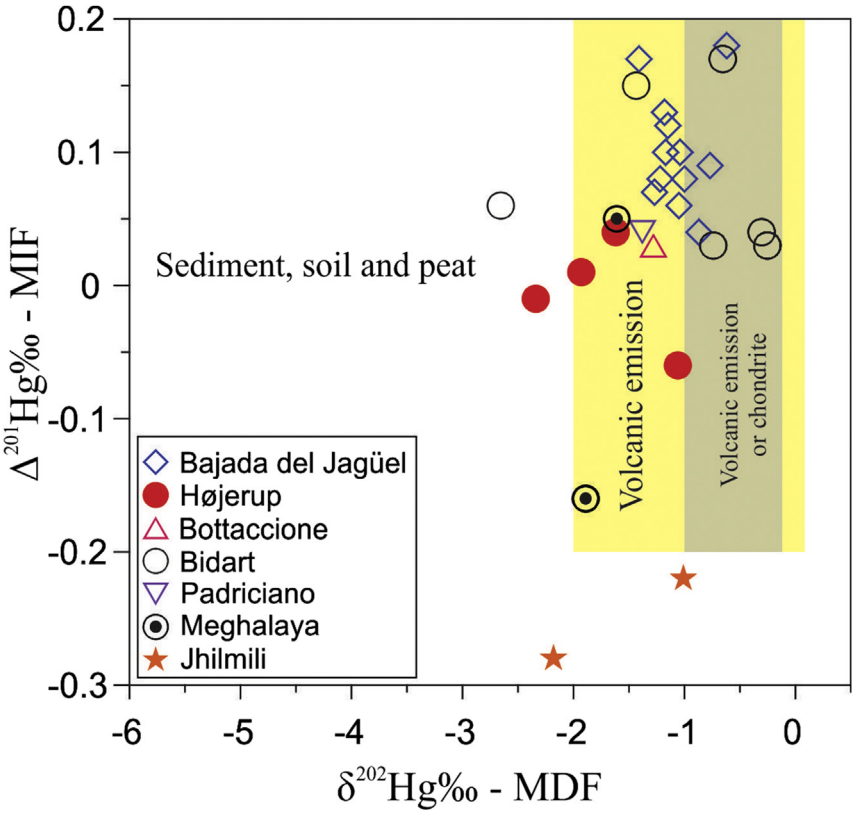

Fig. 11. In a δ^{202}Hg (MDF)–Δ^{201}Hg (MIF) plot, values most samples in this study lie within the range for volcanogenic Hg. Ranges for volcanogenic and chondritic Hg are from Bergquist and Blum (2009) and are shown as vertical bars.

represent a record of the Deccan phase-2 eruptions. One of these spikes is situated within the CF2 foraminiferal biozone (e.g. Meghalaya), within the 250 kyr (beginning of Deccan phase-2) and 160 kyr (CF2–CF1biozones boundary) before the KPg boundary after carbon dioxide, sulfuric aerosols and other toxic agents reached a critical threshold. The second spike, at the KPg boundary, is also coeval to the Deccan phase-2 (e.g. Højerup and Bottaccione) and a third one, within the P1a foraminiferal biozone in the lowermost Danian (e.g. Jhilmili), is likely related to late Deccan phase-2 eruptions (within the 220–500 kyr interval after the KPg boundary). These three periods of anomalous Hg deposition identified here suggest events of enhanced Hg deposition over broad areas of the globe.

b) The possibility that Hg enhancements around the KPg boundary at Højerup, Bottaccione, and Meghalaya, could be postdepostional, resulting from scavenging by anoxia on the seafloor and transported downward into the uppermost 50 cm layer, is not confirmed by the stratigraphic record of Mo/Al redox proxy that does not support a decrease in oxygenation.

(c) Differences in the magnitude of the Hg concentrations among the complete studied sections are due to either difference in sedimentation rates, proximity to the continents, or to the partial leaching of Hg during weathering and/or diagenesis.

(d) In selecting Hg enriched values that may represent true volcanic Hg loading to the environment, it is a common practice to normalize Hg concentrations by the corresponding TOC % values. This approach potentially confirms true Hg enrichments but inaccuracy of measurements may lead to highly variable or unrealistic Hg/TOC spikes in cases where extremely low TOC values (<0.2%) are used (e.g. uppermost Danian portion of the Meghalaya section).

(e) The δ^{202}Hg data for boundary clays or from samples of other sedimentary rocks spanning the KPg boundary lie within the range of volcanogenic Hg. Small and positive Δ^{201}Hg seems to support a long range atmospheric transport of Hg. This indicates a promising start of using Hg isotopes in the identification of the Hg source.

Despite these stimulating results, one cannot assure that Hg is volcanogenic solely based on isotopic similarity because of: (a) limited amount of Hg isotope data, and (b) processes involved as eruption, transportation and even deposition may have lead to Hg isotope fractionation/modification of the original Hg isotope signals.

We hope this study contributes to the growing agreement that a single large asteroid/comet impact could not have been the sole cause of the end-Cretaceous mass extinction, but rather a contributing factor along with volcanism.

Acknowledgments

We thank Gilsa M. Santana and Vilma S. Bezerra for assistance with stable isotope analyses in the LABISE and to Ingra K.C. Belmino for the help with the Hg analyses at the LABOMAR. We acknowledge N. Thibault (Copenhagen) for discussions about stratigraphic details of Danish successions. We are grateful to Prof. Finn Surlyk (University of Copenhagen) and to an anonymous reviewer whose comments and suggestions on an earlier version of the manuscript greatly contributed to improve it. MKP and VCT are grateful to the

Brazilian Council for Scientific and Technological Development (CNPq) for three-month visiting professor fellowships in the LABISE, Brazil. V.C. Tewari is thankful to Dr. A.K. Gupta, Director of WIHG, for collaborative project between this Institution and the NEG–LABISE. Samples from Bidart (6) analyzed for Hg isotopes in this study were provided by Eric Font to whom we are grateful. This study was partially supported by grants from National "973" (2013CB430001), Strategic Priority Research Program of CAS (n. XDB05030302) and NSF China (41273023) to JBC, and to ANS (CNPq grants n. 472842/2010-2 and 471013/2012-9 and FACEPE grants APQ 0727-1.07/08 and APQ-1059-9.05/12) and CNPq grant no. 576.601/2009-1 to LDL. Financial support through the Danish Agency for Science, Technology and Innovation (grant n. 11-103378) to RF and through the Danish National Research Foundation's Center of excellence NordCEE (DNRF grant n. DNRF53) is highly appreciated. This is the NEG–LABISE contribution n. 272.

References

Aberhan, M., Weidemeyer, S., Kiessling, W., Scasso, R.A., Medina, F.A., 2007. Faunal evidence for reduced productivity and uncoordinated recovery in Southern Hemisphere Cretaceous–Paleogene boundary sections. Geology 35, 227–230.

Abrajevitch, A., Font, E., Florindo, F., Roberts, A.P., 2015. Asteroid impact vs. Deccan eruptions: the origin of low magnetic susceptibility beds below the Cretaceous-Paleogene boundary revisited. Earth Planetary Science Letters 430, 209–223.

Aguirre-Urreta, B., Tunik, M., Naipauer, M., Pazos, P., Ottone, E., Fanning, M., Ramos, V.A., 2011. Malargüe group (Maastrichtian–Danian) deposits in the Neuquén Andes, Argentina: implications for the onset of the first Atlantic transgression related to Western Gondwana break-up. Gondwana Research 19, 482–494.

Alvarez, W., 2009. The historical record in the Scaglia limestone at Gubbio: magnetic reversals and the Cretaceous–Tertiary mass extinction. Sedimentology 56, 137–148.

Alvarez, L.W., Alvarez, W., Asaro, F., Michel, H.V., 1980. Extraterrestrial cause for the Cretaceous–Tertiary extinction. Science 208, 1095–1108.

Banerji, R.K., 1981. Cretaceous–Eocene sedimentation, tectonism and biofacies in the Bengal Basin, India. Palaeogeography, Palaeoclimatology, Palaeoecology 34, 57–85.

Berggren, W.A., Kent, D.V., Swisher III, C.C., Aubry, M.P., 1995. A revised Cenozoic geochronology and chronostratigraphy. In: Berggren, W.A., Kent, D.V., Aubry, M.-P., Hardenbol, J. (Eds.), Geochronology, Time Scales and Stratigraphic Correlation, Society of Economic Paleontologists and Mineralogists, Special Volume No. 54, pp. 129–212.

Bergquist, B.A., Blum, J.D., 2009. The odds and evens of mercury isotopes: applications of mass-dependent and mass-independent isotope fractionation. Elements 5, 353–357.

Bertels, A., 1975. Bioestratigrafía del Paleogeno en la República Argentina. Revista Española de Micropaleontologia 8, 429–450.

Bhandari, N., Shukla, P.N., Cini Castognoli, G., 1993. Geochemistry of some K/T sections in India. Palaeogeography, Palaeoclimatology, Palaeoecology 104, 199–211.

Bhandari, N., Gupta, M., Panday, J., Shukla, P.N., 1994. Chemical profiles in K/T boundary section of Meghalaya, India: cometary, asteroidal or volcanic. Chemical Geology 113, 45–60.

Blum, J.D., Sherman, L.S., Johnson, M.W., 2014. Mercury isotopes in earth and environmental sciences. Annual Reviews of Earth Planetary Science 42, 249–269.

Bond, D.P.G., Wignall, P.B., 2014. Large igneous provinces and mass extinctions: an update. Geological Society of America Special Paper 505 29–55.

Bond, D.P.G., Wignall, P.B., Joachimski, M., Sun, Y., Savov, I., Grasby, S.E., Beauchamp, B., Blomeier, D.P.G., 2015. An abrupt extinction in the Middle Permian (Capitanian) of the Boreal Realm (Spitsbergen). Geological Society of America Bulletin. http://dx.doi.org/10.1130/B31216.1.

Bonté, P., Delacotte, O., Renard, M., Laj, C., Boclet, D., Jehanno, C., Rocchia, R., 1984. An iridium rich layer at the Cretaceous Tertiary boundary in the Bidart Section (Southern France). Geophysical Research Letters 11, 473–476.

Caffau, M., Plenicar, M., Pugliese, N., Drobne, K., 1998. Late Maastrichtian rudists and microfossils in the Karst region (NE Italy and Slovenia). Geobios, Memoire Special 22, 37–46.

Callegaro, S., Baker, D.R., De Min, A., Marzoli1, A., Geraki, K., Bertrand, H., Viti, C., Nestola, F., 2014. Microanalyses link sulfur from large igneous provinces and Mesozoic mass extinctions. Geology 42, 895–898.

Casadío, S., 1998. Las ostras del límite Cretácico–Paleógeno de la cuenca Neuquina (Argentina). Su importancia bioestratigráfica y paleobiogeográfica. Ameghiniana 35, 449–471.

Chen, J.-B., Hintelmann, H., Dimock, B., 2010. Chromatographic pre-concentration of Hg from dilute aqueous solutions for isotopic measurement by MC-ICP-MS. Journal of Analytical Atomic Spectrometry 25, 1402–1409.

Chen, J.-B., Hintelmann, H., Feng, X.-B., Dimock, B., 2012. Unusual fractionation of both odd and even mercury isotopes in precipitation from Peterborough, ON, Canada. Geochimica et Cosmochimica Acta 90, 33–46.

Chenet, A.L., Courtillot, V., Fluteau, F., Gerard, M., Quidelleur, X., Khadri, S.F.R., Subbarao, K.V., Thordarson, T., 2009. Determination of rapid Deccan eruptions across the Cretaceous–Tertiary boundary using paleomagnetic secular variation: 2. Constraints from analysis of eight new sections and synthesis for a 3500-m-thick composite section. Journal of Geophysical Research 114, 1–38.

Coccioni, R., Premoli Silva, I., 2015. Revised Upper Albian–Maastrichtian planktonic foraminiferal biostratigraphy and magneto-stratigraphy of the classical Tethyan Gubbio section (Italy). Newsletters on Stratigraphy 48, 47–90.

Coccioni, R., Frontalini, F., Bancalà, G., Fornaciari, E., 2010. The Dan-C2 hyperthermal event at Gubbio (Italy): global implications, environmental effects, and cause(s). Earth and Planetary Science Letters 297 (2010), 298–305.

Cripps, J.A., 2002. Environmental Impact of Deccan Trap Flood Basalt Volcanism: Assessment of Regional Floral Responses to Late Cretaceous–early Tertiary Activity. Ph.D. Thesis, Open University, Milton Keynes, UK, 502 pp.

Drobne, K., Ogorelec, B., Pleničar, M., Barattolo, F., Turnšek, D., Zucchi Stolfa, M.L., 1989. The Dolenja Vas section, a transition from Cretaceous to Palaeocene in the NW Dinarides, Yugoslavia. Memorie – Società Geologica Italiana 40, 73–84.

Estrade, N., Carignan, J., Donard, O.F.X., 2011. Tracing and quantifying anthropogenic mercury sources in soils of northern France using isotopic signatures. Environmental Science and Technology 45, 1235–1242.

Font, E., Fabre, F., Nédélec, A., Adatte, T., Keller, G., Veiga-Pires, C., Ponte, J., Mirão, José, Khozyem, H., Spangenberg, J., 2014. Atmospheric halogen and acid rains during the main phase of Deccan eruptions: magnetic and mineral evidence. Geological Society of America Special paper 505 1–16.

Font, E., Adatte, T., Sial, A.N., Lacerda, L.D., Keller, G., Punekar, J., 2016. Mercury anomaly, Deccan volcanism and the end-Cretaceous mass extinction. Geology 44, 171–174.

Foucher, D., Ogrinc, N., Hintelmann, H., 2009. Tracing mercury contamination from the Idrija mining region (Slovenia) to the Gulf of Trieste using Hg isotope ratio measurements. Environmental Science & Technology 43, 33–39.

Galbrun, B., Gardin, S., 2004. New chronostratigraphy of the Cretaceous-Paleogene boundary interval at Bidart (France). Earth and Planetary Science Letters 224, 19–32.

Galeotti, S., Moretti, M., Cappelli, C., Phillips, J., Lanci, L., Littler, K., Monechi, S., Petrizzo, M.R., Premoli Silva, I., Zachos, J.C., 2015. The Bottaccione section at Gubbio, central Italy: a classical Paleocene Tethyan setting revisited. Newsletters on Stratigraphy 48, 325–339.

Garg, R., Khowaja-Ateequzzaman, Prasad, V., 2006. Significant dinoflagellate cyst Biohorizons in the Upper Cretaceous–Palaeocene succession of the Khasi Hills, Meghalaya. Journal Geological Society India 67, 737–747.

Gehrke, G.E., Blum, J.D., Marvin-DiPasquale, M., 2011. Sources of mercury to San Francisco Bay surface sediment as revealed by mercury stable isotopes. Geochimica et Cosmochimica Acta 75, 691–705.

Gertsch, B., Keller, G., Adatte, T., Garg, R., Prasad, V., Berner, Z., Fleitmann, D.S., 2011. Environmental effects of Deccan volcanism across the Cretaceous–Tertiary transition in Meghalaya, India. Earth and Planetary Science Letters 310, 272–285.

Grasby, S.E., Sanei, H., Beauchamp, B., Chen, Z., 2013. Mercury deposition through the Permo–Triassic Biotic Crisis. Chemical Geology 351, 209–216.

Grasby, S.E., Beauchamp, B., Bond, D.P.G., Wignall, P.B., Sanei, 2015a. Mercury anomalies associated with three extinction events (Capitanian Crisis, Latest Permian Extinction and the Smithian/Spathian Extinction) in NW Pangea. Geological Magazine. http://dx.doi.org/10.1017/S0016756815000436.

Grasby, S.E., Beauchamp, B., Bond, D.P.G., Wignal, P., Talavera, C., Galloway, J.M., Piepjohn, K., Reinhardt, L., Blomeier, D., 2015b. Progressive environmental deterioration in northwestern Pangea leading to the latest Permian extinction. Geological Society of America Bulletin 127, 1311–1347.

Gregorič, M., Caffau, M., Lenaz, D., De Min, A., 1998. Late Maastrichitian–Palaeocene unaltered glassy microspherules at Padriciano, Trieste Karst, NE Italy: a preliminary report. Razprave 4, Razreda SAZU 211–233.

Grotzinger, J.P., Fike, D.A., Fischer, W.W., 2011. Enigmatic origin of the largest known carbon isotope excursion in Earth's history. Nature Geosciences 4, 285–292.

Habib, D., Saeedi, F., 2007. The Manumiella seelandica global spike: cooling during regression at the close of the Maastrichtian. Palaeogeography, Palaeoclimatology, Palaeoecology 255, 87–97.

Hansen, T., Surlyk, F., 2014. Marine macrofossil communities in the uppermost Maastrichtian chalk of Stevns Klint, Denmark. Palaeogeography, Palaeoclimatology, Palaeoecology 399, 323–344.

Hansen, H.J., Toft, P., 1996. Dolenja Vas and its carbon isotopes. In: Drobne, K., Gorican, S., Kotnik, B. (Eds.), Int. Workshop Postojna'96. The Role of Impact Processes in the Geological and Biological Evolution of Planet Earth, pp. 31–32.

Hansen, H.J., Drobne, K., Gwozda, R., 1995. The K/T boundary in Slovenia: dating by magnetic susceptibility stratigraphy and an iridium anomaly in a debris flow. In: Montanari, A., Coccioni, R. (Eds.), 4th International Workshop ESF Sci. Network "Impact Cratering and Evolution of Planet Earth", Ancona. The Role of Impacts on the Evolution of the Atmosphere and Biosphere with Regard to Shortand Long-Term Changes. Abstract and Field Trips, pp. 81–82.

Hart, M.B., Feist, S.E., Price, G.D., Leng, M.J., 2004. Reappraisal of the K–T boundary succession at Stevns Klint, Denmark. Journal of the Geological Society of London 161, 1–8.

Heredía, S., Salgado, L., 1999. Posición estratigráfica de los estratos supracretácicos portadores de dinosaurios en Lago Pellegrini, Patagonia Septentrional, Argentina. Ameghiniana 36, 229–234.
Hildebrand, A.R., Boynton, W.V., 1989. Hg anomalies at the K/T boundary: evidence for acid rain? Meteoritics 24, 277–278.
Howell, J.A., Schwarz, E., Spalletti, L.A., Veiga, G.D., 2005. The Neuquén Basin: an overview. In: Veiga, G.D., Spalletti, L.A., Howell, J.A., Schwarz, E. (Eds.), The Neuquén Basin, Argentina: A Case Study in Sequence Stratigraphy and Basin Dynamics, Geological Society, London, Special Publications, 252, pp. 1–14.
Hsü, K.J., McKenzie, J.A., 1985. A "Strangelove" ocean in earliest Tertiary. In: Sundquist, E.T., Broecker, W.S. (Eds.), Carbon Cycle and Atmosphere CO_2 Natural Variations Archean to Present. Washington, D.C., American Geophysical Union, Geophysical Monograph, 32, pp. 487–492.
Huang, Q., Liu, Y.-L., Chen, J.-B., Feng, X.-B., Huang, W.-L., Yuan, S.-L., Cai, H.-M., Fu, X.-W., 2015. An improved dual-stage protocol to pre-concentrate mercury from airborne particles for precise isotopic measurement. Journal of Analytical Atomic Spectrometry 30, 957–966.
Jiskra, M., Wiederhold, J.G., Bourdon, B., Kretzschmar, R., 2012. Solution and speciation controls of mercury isotope fractionation of Hg(II) sorption to goethite. Environmental Science and Technology 46, 6654–6662.
Jourdan, F., Hodges, K., Sell, B., Schaltegger, U., Wingate, M.T.D., Evins, L.Z., Soderlund, U., Haines, P.W., Phillips, D., Blenkinsop, T., 2014. High-precision dating of the Kalkarindji large igneous province, Australia, and synchrony with the Early–Middle Cambrian (Stage 4–5) extinction. Geology 42, 543–546.
Keller, G., Kerr, A.C., 2014. Foreword. In: Keller, G., Kerr, A.C. (Eds.), Volcanism, Impacts, and Mass Extinctions: Causes and Effects, Geological Society of America Special Paper, 505, pp. v–ix.
Keller, G., Adatte, T., Tantawy, A.A., Berner, Z., Stinnesbeck, W., Stueben, D., Leanza, H.A., 2007. High stress late Maastrichtian and early Danian palaeoenvironment in the Neuquén Basin, Argentina. Cretaceous Research 28, 939–960.
Keller, G., Adatte, T., Gardin, S., Bartolini, A., Bajpai, S., 2008. Main Deccan volcanism phase ends near the K–T boundary: evidence from the Krishna–Godavari Basin, SE India. Earth Planetary Science Letters 268, 293–311.
Keller, G., Khosla, S.C., Sharma, R., Khosla, A., Bajpai, S., Adatte, T., 2009. Early Danian Planktic foraminifera from intertrappean beds at Jhilmili, Chhindwara District, Madhya Pradesh, India. Journal of Foraminifer Research 39, 40–55.
Keller, G., Bhowmick, P.K., Upadhyay, H., Dave, A., Reddy, A.N., Jaiprakash, B.C., Adatte, T., 2011. Deccan volcanism linked to the Cretaceous-Tertiary boundary mass extinction: new evidence from ONGC wells in the Krishna-Godavari Basin. Journal of the Geological Society of India 78, 399–428.
Keller, G., Adatte, T., Bhowmick, P.K., Upadhyay, H., Dave, A., Reddy, A.N., Jaiprakash, B.C., 2012. Nature and timing of extinctions in Cretaceous–Tertiary planktic foraminifera preserved in Deccan intertrappean sediments of the Krishna-Godavari Basin, India. Earth Planetary Science Letters 341, 211–221.
Keller, G., Punekar, J., Mateo, P., 2016. Upheavals during the Late Maastrichtian: volcanism, climate and faunal events preceding the end-Cretaceous mass extinction. Palaeogeography, Palaeoclimatology, Palaeoecology 441, 137–151.
Knoll, A.H., Hayes, J.M., Kaufman, A.J., Swett, K., Lambert, I.B., 1986. Secular variation in carbon isotope ratios from upper Proterozoic successions of Svalbard and East Greenland. Nature 321, 832–838.
Korte, C., Kozur, H.W., 2010. Carbon-isotope stratigraphy across the Permian–-Triassic boundary: a review. Journal of Asian Earth Sciences 39, 215–235.
Krishnan, M.S., 1968. Geology of India and Burma. In: Krishnan, M.S. (Ed.), Madras, 536 pp.
Krupp, R., 1988. Physicochemical Aspects of Mercury Metallogenesis. Chemical Geology 69, 345–356.
Laffont, L., Sonke, J.E., Maurice, L., Hintelmann, H., Sanchez-Baccarez, Y., Perez, T., Behra, P., 2009. Anomalous mercury isotopic compositions of fish and human hair in the Bolivian Amazon. Environmental Science and Technology 43, 8985–8990.
Laffont, L., Sonke, J.E., Maurice, L., Monroy, S.L., Chincheros, J., Amouroux, D., Behra, P., 2011. Hg speciation and stable isotope signatures in human hair as a tracer for dietary and occupational exposure to mercury. Environmental Scienceand Technology 45, 9910–9916.
Lauridsen, B.W., Bjerager, M., Surlyk, F., 2012. The middle Danian Faxe Formation – new lithostratigraphic unit and a rare taphonomic window into the Danian of Denmark. Bulletin of the Geological Society of Denmark 60, 47–60.
Legarreta, L., Uliana, M.A., 1999. El Jurásico y Cretácico de la Cordillera Principal y la Cuenca Neuquina. In: Caminos, R. (Ed.), Geología Argentina, Servicio Geológico Minero Argentino, Anales 29, 16, pp. 399–416.
Legarreta, L., Kokogián, D.A., Boggetti, D.A., 1989. Depositional sequences of the Malargüe group (Upper Cretaceous–Lower Tertiary), Neuquén Basin, Argentina. Cretaceous Research 10, 337–356.
Lowrie, W., Alvarez, W., Asaro, F., 1990. The origin of the white beds below the Cretaceous Tertiary boundary in the Gubbio section, Italy. Earth Planetary Science Letters 98, 303–331.
Luterbacher, H.P., Premoli Silva, I., 1964. Biostratigrafia del limite Cretaceo–Terziario nell'Appennino centrale. Rivista Italiana di Paleontologia e Stratigrafia 70, 67–128.
Lyons, T.W., Werne, J.P., Hollander, D.J., Murray, R.W., 2003. Contrasting sulfur geochemistry and Fe/Al and Mo/Al ratios across the last oxic-to-anoxic transition in the Cariaco Basin, Venezuela. Chemical Geology 195, 131–157.
Maloof, A.C., Porter, S.M., Moore, J.H., Dudás, F.O., Bowring, S.A., Higgins, J.A., Fike, D.A., Michael, Eddy, P., 2010. The earliest Cambrian record of animals and ocean geochemical change. Geological Socity of America Bulletin 122, 1731–1774.
Martínez-Cortizas, A., Pontevedra-Pombal, X., García-Rodeja, E., Nóvoa-Muñoz, J.C., Shotyk, W., 1999. Mercury in a Spanish Peat Bog: archive of climate change and atmospheric metal deposition. Science 284, 939–942.
Marton, E., Drobne, K., Cimerman, F., Ćosović, V., Košir, A., 1995. Paleomagnetism of latest Maastrichtian through Oligocene rocks in Istria (Croatia), the Karst region, and S of the Sava fault (Slovenia). In: Vlahović, I., Velić, I., Šparica, M. (Eds.), Proc.1st Croatian Geological Congress, Zagreb, 2, pp. 355–360.
McLean, D.M., 1985. Deccan Traps mantle degassing in the terminal Cretaceous marine extinctions. Cretaceous Research 6, 235–259.
Meier, M.M.M., Cloquet, C., Marty, B., Ferrière, L., Koeberl, C., 2015. Hg isotopes at the K-Pg boundary. Goldschmidt Conference, Prague, 16–21 August 2015, p. 1720.
Meyer, K.M., Yu, M., Lehrmann, D., van de Schootbrugge, B., Payne, J.L., 2013. Constraints on early Triassic carbon cycle dynamics from paired organic and inorganic carbon isotope records. Earth Planetary Science Letters 361, 429–435.
Mukhopadhyay, S.K., 2008. Planktonic foraminiferal succession in late Cretaceous to early Paleocene strata in Meghalaya, India. Lethaia 41, 71–84.
Musso, T., Concheyro, A., Pettinari, G., 2012. Clay mineralogy and calcareous nannofossils from Jagüel and Roca formations in the eastern sector of Pellegrini Lake, Neuquén Basin, República Argentina. Andean Geology 393, 511–540.
Nagappa, Y., 1959. Foraminiferal biostratigraphy of the Cretaceous: Eocene succession in the India–Pakistan–Burma region. Micropaleontology 5, 145–192.
Nañez, C., Concheyro, A., 1997. Límite Cretácico–Paleogeno. In: Geología y Recursos Minerales del Departamento Anelo, Provincia de Neuquén, República Argentina. Dirección Nacional del Servicio Geológico, Anales 25 y Dirección Provincial de Minería Boletín, 3, pp. 12–49.
Nañez, C., Parras, A., Hansen, H.J., Concheyro, A., Alonso, S., Lojen, S., Pires, M., 2002. A southern, shallow marine, Cretaceous–Paleogene boundary: Bajada del Jagüel Basin, Argentina. GAC–MAC Annual Joint Meeting, Saskatoon, Abstracts 27, 79.
Nascimento-Silva, V.M., Sial, A.N., Ferreira, V.P., Neumann, V.H., Barbosa, J.A., Pimentel, M.M., Lacerda, L.D., 2011. Cretaceous–Paleogene transition at the Paraíba Basin, northeastern, Brazil: carbon-Isotope and mercury subsurface stratigraphies. Journal of South American Earth Sciences 32, 379–392.
Nascimento-Silva, M.V., Sial, A.N., Ferreira, V.P., Barbosa, J.A., Neumann, V.H., Pimentel, M.M., Lacerda, L.D., 2013. Carbon isotopes, rare-earth elements and mercury behavior of Maastrichtian–Danian carbonate succession of the Paraíba Basin, Northeastern Brazil. In: Bojar, A.V., Melinte-Dobrinescu, M.C., Smit, J. (Eds.), Isotopic Studies in Cretaceous Research, Geological Society, London, Special Publications, 382, pp. 85–104.
Oehlert, A.M., Swart, P.K., 2014. Interpreting carbonate and organic carbon isotope covariance in the sedimentary record. Nature Communications. http://dx.doi.org/10.1038/ncomms5672.
Ogorelec, B., Dolenec, T., Cucchi, F., Giacomich, R., Drobne, K., Pugliese, N., 1995. Sedimentological and geochemical character- istics of carbonate rocks from the K/T Boundary to lower Eocene in the Karst area (NW Adriatic Platform). 1st Croatian Geological Congress, Opatija 415–421.
Outridge, P.M., Sanei, H., Stern, G.A., Hamilton, P.B., Goodarzi, F., 2007. Evidence for control of mercury accumulation in sediments by variations of aquatic primary productivity in Canadian High Arctic lakes. Environmental Science & Technology 41, 5259–5265.
Pal, S., Shrivastava, J.P., Mukhopadhyay, S.K., 2015. Polycyclic aromatic hydrocarbon compound excursions and K/Pg transition in the late Cretaceous–early Palaeogene succession of the Um Sohryngkew river section, Meghalaya. Current Science 29, 1140–1149.
Palamarczuk, S., Habib, D., 2001. Dinoflagellate evidence of the Cretaceous–Paleogene Boundary in Argentina. Geological Society of America, Annual Meeting, Nov. 5–8.
Palamarczuk, S., Habib, D., Olsson, R.K., Hemming, S., 2002. The Cretaceous–Paleogene boundary in Argentina: new evidence from dinoflagellate, foraminiferal and radiometric dating. Geological Society of America Abstracts with Program. No. 61–20.
Palinkaš, A.L., Drobne, K., Durn, G., Miko, S., 1996. Mercury anomaly at the Cretaceous–Tertiary boundary: Dolenja Vas, Slovenia. In: Drobne, K., Goričan, Š., Kotnik, B. (Eds.), Int. Workshop Postojna '96. The Role of Impact Processes in the Geological and Biological Evolution of Planet Earth, 31–32.
Pandey, J., 1990. Cretaceous/Tertiary boundary, iridium anomaly, and foraminifer breaks in the Um Sohryngkew river section, Meghalaya. Current Science 59, 570–575.
Papú, O.H., Prámparo, M.B., Nañez, C., Concheyro, A., 1999. Palinología y micropaleontología de la Formación Jagüel (Maastrichtiano-Daniano), perfil Opazo, cuenca Neuquina, Argentina. Simposio Paleógeno de América del Sur. Actas Servicio Geológico Minero Argentino, Anales 33, 17–31.
Pardo, A., Keller, G., 2008. Biotic effects of environmental catastrophes at the end of the Cretaceous and early Tertiary: Guembelitria and Heterohelix blooms. Cretaceous Research 29, 1058–1073.
Percival, L.M.E., Witt, M.L.I., Mather, T.A., Hermoso, M., Jenkyns, H.C., Hesselbo, S.P., Al-Suwaidi, A.H., Storm, M.S., Xu, W., Ruhl, M., 2015. Globally enhanced mercury deposition during the end-Pliensbachian extinction and Toarcian OAE: a link to the Karoo–Ferrar large igneous province. Earth and Planetary Science Letters 428, 267–280.
Premoli Silva, I., Sliter, W.V., 1994. Cretaceous planktonic foraminiferal biostratrigraphy and evolutionary trends from the Bottacioine section, Gubbio, Italy. Palaeontographica Italica 82, 1–89.

Pugliese, N., Drobne, K., Barattolo, F., Caffau, M., Galvani, R., Kedves, M., Montenegro, M.E., Pirini-Radrizzani, C., Pleničar, M., Turnšek, D., 1995. Micro- and macrofossils from K/T boundary through Paleocene in the Northern Adriatic Platform. In: Vlahović, I., Velić, I., Šparica, M. (Eds.), Proceedings 2, 1st Croatian Geol. Congress Opatija. Inst. Geol., Zagreb, 505–513.

Pugliese, N., Arbulla, D., Caffau, M., Drobne, K., 2000. Strategia di vita nel biota daniano (SBZ 1) del Carso Triestino (Italia). Accademia Nazionale de Scienze Lett. Arti di Modena. Collana di Studi 21, 215–220.

Punekar, A., Mateo, P., Keller, G., 2014. Effects of Deccan volcanism on paleoenvironment and planktic foraminifera: a global survey. Geological Society of America Special Papers 505, 91–116.

Pyle, D.M., Mather, T.A., 2003. The importance of volcanic emissions for the global atmospheric mercury cycle. Atmospheric Environment 37, 5115–5124.

Raja Rao, C.S., Sahasrabudhe, S.S., Deshmukh, S.S., Raman, R., 1999. Distribution, structure and petrography of the Deccan traps, India. In: Subbarao, K.V. (Ed.), Deccan Volcanic Province, Memoir — Geological Society of India, 43, pp. 401–414.

Rasmussen, J.A., Heinberg, C., Hankasson, E., 2005. Planktonic foraminifers, biostratigraphy and the diachronous nature of the lowermost Danian Cerithium limestone at Stevns Klint, Denmark. Bulletin of the Geological Society Denmark 52, 113–131.

Renne, P.R., Deino, A.L., Hilgen, F.J., Kuiper, D.F., Mark, D.F., Mitchell 3rd, W.S., Morgan, E., Mundil, R., Smit, J., 2013. Time scales of critical events around the Cretaceous–Paleogene boundary. Science 339, 684–687.

Roos-Barraclough, F., Shotyk, W., 2003. Millennial-scale records of atmospheric mercury deposition obtained from ombrotrophic and minerotrophic peatlands in the Swiss Jura Mountains. Environmental Science & Technology 37, 235–244.

Roos-Barraclough, F., Martinez-Cortizas, A., García-Rodeja, E., Shotyk, W., 2002. A 14,500 year record of the accumulation of atmospheric mercury in peat: volcanic signals, anthropogenic influences and a correlation to bromine accumulation. Earth and Planetary Science Letters 202, 435–451.

Sanei, H., Grassby, S.E., Beauchamp, B., 2012. Latest Permian mercury anomalies. Geology 40, 63–66.

Sanei, H., Outridge, P.M., Stern, G.A., Macdonald, R.W., 2014. Classification of mercury-labile organic matter relationships in lake sediments. Chemical Geology 373, 87–92.

Santos, G.M., Cordeiro, R.C., Silva Filho, E.V., Turcq, B., Lacerda, L.D., Fifield, L.K., Gomes, P.R.S., Hauscaden, P.A., Sifeddine, A., Albuquerque, A.L.S., 2001. Chronology of the atmospheric mercury in Lagoa da Pata Basin, Upper Rio Negro of Brazilian Amazon. Radiocarbon 43, 801–808.

Scasso, R., Concheyro, A., Kiessling, W., Aberhan, M., Hecht, L., Medina, F., Tagle, R., 2005. A tsunami deposit at the Cretaceous/Paleogene boundary in the Neuquén Basin of Argentina. Cretaceous Research 26, 283–297.

Schoene, B., Samperton, K.M., Eddy, M.P., Keller, G., Adatte, T., Bowring, S., Khadri, F.R., Gertsch, B., 2015. U–Pb geochronology of the Deccan Traps and relation to the end-Cretaceous mass extinction. Science 347, 182–184.

Schroeder, W.H., Munthe, J., 1998. Atmospheric mercury – an overview. Atmospheric Environment 32, 809–822.

Schuster, P.F., Krabbenhoft, D.P., Naftz, D.L., Cecil, L.D., Olson, M.L., Dewild, J.F., Susong, D.D., Green, J.R., Abbott, M.L., 2002. Atmospheric mercury deposition during the last 270 years: a glacial ice core record of natural and anthropogenic sources. Environmental Science & Technology 36, 2303–2310.

Scotese, C.R., 2013. Map Folio 16, KT Boundary (65.5 Ma, latest Maastrichtian), PALEOMAP PaleoAtlas for ArcGIS, vol. 2. Cretaceous, PALEOMAP Project, Evanston, IL.

Self, S., Jay, A.E., Widdowson, M., Keszthelyi, L.P., 2008. Correlation of the Deccan and Rajahmundry Trap lavas: are these the longest and largest lava flows on Earth? Journal of Volcanology and Geothermal Research 172, 3–19.

Serra-Kiel, J., Hottinger, L., Caus, E., Drobne, K., Ferrandez, C., Jauhri, A.K., Less, G., Pavlovec, R., Pignatti, J., SAmsó, J.M., Schaub, H., Sirel, E., Strougo, A., Tambareau, Y., Tospquella, J., Zakrebskaya, E., 1998. Larger foraminiferal biostratigraphy of the Tethyan Paloecene and Eocene. Bulletin de la Societé Geologique de France 169, 281–299.

Sherman, L.S., Blum, J.D., Johnson, K.P., Keeler, G.J., Barres, J.A., Douglas, T.A., 2010. Mass-independent fractionation of mercury isotopes in Arctic snow driven by sunlight. Nature Geosciences 3, 173–177.

Shukla, U.K., Srivastava, R., 2008. Lizard eggs from Upper Cretaceous Lameta Formation of Jabalpur, central India, with interpretation of depositional environments of the nest-bearing horizon. Cretaceous Research. http://dx.doi.org/10.1016/j.cretres.2008.02.003.

Sial, A.N., Gaucher, C., Silva Filho, M.A., Ferreira, V.P., Pimentel, M.M., Lacerda, L.D., Silva Filho, E.V., Cezario, W., 2010. C-, Sr-isotope and Hg stratigraphies of Neoproterozoic cap carbonates of the Sergipano Belt, Northeastern Brazil. Precambrian Research 182, 351–372.

Sial, A.N., Lacerda, L.D., Ferreira, V.P., Frei, R., Marquillas, R.A., Barbosa, J.A., Gaucher, C., Windmöller, C.C., Pereira, N.S., 2013. Mercury as a proxy for volcanic activity during extreme environmental turnover: the Cretaceous–Paleogene transition. Palaeogeography, Palaeoclimatology, Palaeoecology 387, 153–164.

Sial, A.N., Chen, J.-B., Lacerda, L.D., Peralta, S., Gaucher, C., Frei, R., Cirilli, S., Ferreira, V.P., Marquillas, R.A., Barbosa, J.A., Pereira, N.S., Belmino, I.K.C., 2014. High-resolution Hg Chemostratigraphy: a contribution to the distinction of chemical fingerprints of the Deccan volcanism and Cretaceous–Paleogene boundary impact event. Palaeogeography, Palaeoclimatology, Palaeoecology 414, 98–115.

Sonke, J.E., Blum, J.D., 2013. Advances in mercury stable isotope biogeochemistry. Chemical Geology 336, 1–4.

Sonke, J.E., Schaefer, J., Chmeleff, J., Audry, S., Blanc, G., Dupré, B., 2010. Sedimentary mercury stable isotope records of atmospheric and riverine pollution from two major European heavy metal refineries. Chemical Geology 279, 90–100.

Stern, G.A., Sanei, H., Roach, P., Delaronde, J., Outridge, P.M., 2009. Historical interrelated variations of mercury and aquatic organic matter in lake sediment cores from a subarctic lake in Yukon, Canada: further evidence toward the algal-mercury scavenging hypothesis. Environmental Science & Technology 43, 7684–7690.

Sun, R., Heimbürger, L.E., Sonke, J.E., Liu, G., Amouroux, D., Berail, S., 2013. Mercury stable isotope fractionation in six utility boilers of two large coal-fired power plants. Chemical Geology 336, 103–111.

Surlyk, F., 1997. A cool-water carbonate ramp with bryozoans mounds: Late Cretaceous–Danian of the Danish Basin. In: James, N.P., Clarke, J.D.A. (Eds.), Cool Water Carbonates, S.E.P.M. Special Publication, vol. 56, pp. 293–307.

Surlyk, F., Damholt, T., Bjerager, M., 2006. Stevns Klint, Denmark: Uppermost Maastrichtian chalk, Cretaceous–Tertiary boundary, and lower Danian bryozoans mound complex. Bulletin of the Geological Society of Denmark 54, 1–48.

Surlyk, F., Rasmussen, S.L., Boussaha, M., Schiøler, P., Schovsbo, N.H., Sheldon, E., Stemmerik, L., Thibault, N., 2013. Upper Campanian–Maastrichtian holostratigraphy of the eastern Danish Basin. Cretaceous Research 46, 232–256.

Svensen, H., Planke, S., Polozov, A.G., Schmidbauer, N., Corfu, F., Podladchikov, Y.Y., Jamtveit, B., 2009. Siberian gas venting and the end-Permian environmental crisis. Earth and Planetary Science Letters 277, 490–500.

Tewari, V.C., Stenni, B., Pugliese, N., Drobne, K., Riccamboni, R., Dolenec, T., 2007. Peritidal sedimentary depositional facies and carbon isotope variation across K/T boundary carbonates from NW Adriatic platform. Palaeogeography, Palaeoclimatology, Palaeoecology 255, 64–76.

Tewari, V.C., Lokho, K., Kumar, K., Siddaiah, N.S., 2010a. Late Cretaceous–Paleocene Basin architecture and evolution of the Shillong Shelf sedimentation, Meghalaya, Northeast India. Journal of Indian Geological Congress 22, 61–73.

Tewari, V.C., Kumar, K., Lokho, K., Siddaiah, N.S., 2010b. Lakadong Limestone: Paleocene-Eocene boundary carbonate sedimentation in Meghalaya, northeastern India. Current Science 98, 88–94.

Thibault, N., Harlou, R., Schovsbo, N.H., Stemmerik, L., Surlyk, F., 2015. Late Cretaceous (Late Campanian–Maastrichtian) sea surface temperature record of the Boreal Chalk Sea. Climate of the Past Discussion 11, 5049–5071. http://dx.doi.org/10.5194/cpd-11-5049-2015.

Uliana, M.A., Biddle, K.T., 1988. Mesozoic–Cenozoic paleogeographic and geodynamic evolution of southern South America. Revista Brasileira de Geociencias 18, 172–190.

Vandal, G.M., Fitzgerald, W.F., Boutron, C.F., Candelon, J.P., 1993. Variations in mercury deposition to Antarctica over the past 34,000 years. Nature 362, 621–623.

Vergani, G.D., Tankard, A.J., Belotti, H.J., Welsink, H.J., 1995. Tectonic evolution and paleogeography of the Neuquén Basin, Argentina. In: Tankard, A.J., Suárez Soruco, R., Welsink, H.J. (Eds.), Petroleum Basins of South America, American Association of Petroleum Geologists Memoirs, 62, pp. 383–402.

Wilde, P., Lyons, T.W., Quinby-Hunt, M.S., 2004. Organic carbon proxies in black shales: molybdenum. Chemical Geology 206, 167–176.

Witt, M.L.I., Mather, T.A., Pyle, D.M., Aiuppa, A., Bagnato, E., Tsanev, V.I., 2008. Mercury and halogen emissions from Masaya and Telica volcanoes, Nicaragua. Journal of Geophysical Research, Solid Earth 113, B06203. http://dx.doi.org/10.1029/2007JB005401.

Zambardi, T., Sonke, J.E., Toutain, J.P., Sortinob, F., Shinoharac, H., 2009. Mercury emissions and stable isotopic compositions at Vulcano Island (Italy). Earth and Planetary Science Letters 277, 236–243.